Biogeosciences Discuss., doi:10.5194/bg-2016-215, 2016
Manuscript under review for journal Biogeosciences
Published: 8 June 2016

Biogeosciences Discussions Open Access EGU

Bioavailable atmospheric phosphorous supply to the global ocean: a 3-D global modelling study

Stelios Myriokefalitakis[1], Athanasios Nenes[2,3,4,5], Alex R. Baker[6], Nikolaos Mihalopoulos[1,5] and Maria Kanakidou[1]

[1]Environmental Chemical Processes Laboratory, Department of Chemistry, University of Crete, P.O. Box 2208, 70013 Heraklion, Greece
[2]Institute of Chemical Engineering Sciences (ICE-HT), FORTH, P.O. Box 1414, 26504 Patras, Greece
[3]School of Earth and Atmospheric Sciences, Georgia Institute of Technology, 311 Ferst Drive, Atlanta, GA 30332-0100, USA
[4]School of Chemical and Biomolecular Engineering, Georgia Institute of Technology, 311 Ferst Drive, Atlanta, GA 30332-0100, USA
[5]National Observatory of Athens, Institute for Environmental Research and Sustainable Development, Athens
[6]Centre for Ocean and Atmospheric Science, School of Environmental Sciences, University of East Anglia, Norwich UK, NR4 7TJ

Correspondence to: Stelios Myriokefalitakis (stelios@uoc.gr); Maria Kanakidou (mariak@uoc.gr)

Abstract. The atmospheric cycle of phosphorus (P) is here parameterized in a global 3-D chemistry-transport model, taking into account primary emissions of total P (TP) and dissolved P (DP) associated with mineral dust, combustion particles of natural and anthropogenic sources, bioaerosols, sea-spray and volcanic aerosols. Global TP emissions are calculated to amount roughly 1.33 Tg-P yr^{-1} with mineral sources (about 1.10 Tg-P yr^{-1}) contributing more than 80% to these emissions. Additionally, under acidic atmospheric conditions, for the present study we take into account the P mobilization from mineral dust, that is calculated to contribute about one third (0.14 Tg-P yr^{-1}) to the global DP atmospheric source. The calculated global annual DP deposition flux equals to 0.43 Tg-P yr^{-1} (about 40% enters the ocean), and shows a strong spatial and temporal variability. Considering that all bioaerosol P is bioavailable (BP) and accounting for all other sources of DP, a flux of 0.16 Tg-P yr^{-1} BP to the ocean is derived. Present day simulations of atmospheric P aerosol concentrations and deposition fluxes are satisfactory compared with available observations, indicating however a 50% uncertainty of current knowledge on primary and secondary sources of P that drive its atmospheric cycle. Sensitivity simulations using preindustrial (year 1850) and future (2100) anthropogenic and biomass burning emission scenarios, showed a present-day increase of 75% in the dissolution flux of P present in dust aerosol compared to the 1850 dissolution flux due to increasing atmospheric acidity over the last 150 years. Future reductions in air pollutants, due to the implementation of air-quality regulations, are expected to decrease P mobilization flux by about 30% for the year 2100 compared to the present-day. A striking result is that more than 50% of the BP deposition flux to the ocean originates from biological particle and this contribution is found to maximize in summer when atmospheric deposition impact on the marine ecosystem is the highest due to ocean stratification. These findings reveal the largely unknown but important role of terrestrial bioaerosols as suppliers of bioavailable P to the ocean – with very important implications for past and future responses of ecosystems to global change. Therefore, our study provides new insights to the atmospheric P cycle by demonstrating that bioaerosols are as important carriers of bioavailable P as dust aerosol, that was up to now considered as the only large source of DP external to the open ocean.

Biogeosciences Discuss., doi:10.5194/bg-2016-215, 2016
Manuscript under review for journal Biogeosciences
Published: 8 June 2016

1 Introduction

Phosphorus (P) is an ubiquitous element found in amino-acids, in proteins and as an integral part of organisms together with nitrogen (N) and iron (Fe). It is an essential nutrient that can limit primary production and nitrogen-fixation in aquatic environments and thus significantly influence carbon-storage (Elser et al., 2007). Reviewing experimental data, Moore et al. (2013) proposed two broad regimes of phytoplankton nutrient limitation in the modern upper ocean: 1) N-limited regimes in most of the low latitude oceanic surface and 2) Fe-limitation where subsurface nutrient supply is enhanced; while P may co-limit primary productivity. Moutin et al. (2008) pointed out the potential importance of phosphate for N_2 fixation in particular in the Southeast Pacific under high temperature conditions and Fe availability, favorable for the presence of N_2-fixing organisms (like *Trichodesmium* spp.) that potentially counteract the N-limitation (Deutsch et al., 2007).

The two external-to-the-ocean sources of nutrients are the atmosphere and rivers. Depending on these inputs and marine dynamics, different nutrients can limit the marine primary productivity. Riverine inputs of nutrients to the marine ecosystem are important for coastal regions, while the atmospheric deposition of nutrients is a more significant source to the open ocean (Jickells, 2005; Duce et al., 2008; Mahowald et al., 2008). In contrast to the atmospheric reactive N pool, the atmospheric soluble-P pool is less studied and remains highly uncertain. Okin et al. (2011) evaluated the impact of Fe and P atmospheric deposition to the ocean in increasing N_2-fixation and found that Fe deposition is more important than P deposition in supporting N_2-fixation, while they pointed out the large uncertainty in the bioavailability of atmospherically deposited P. Benitez-Nelson (2000) review discussed the importance of discrete pulses of P input to the oligotrophic seas that have been found to increase the phytoplankton biomass over short timescales. They also estimated that atmospheric P deposition could be underestimated by as much as 50%, when neglecting the P fraction that is soluble under acidic and high temperatures conditions.

In a marine ecosystem not all of P input is directly biologically available to the organisms, however the bioavailability is found to depend on the degree of P solubility (Anderson et al., 2010). Experimentally, the bioavailable P is usually considered to be the “filterable” reactive or total reactive P that passes through a 0.45 μm membrane (Maher and Woo, 1998 and references therein). For marine microorganisms, phosphate is considered as the most bioavailable form of P (Björkman and Karl, 2003), although experiments have shown that human-produced P-containing organics, such as organophosphorus pesticide breakdown products, can also be utilized by bacteria (Cook et al., 1978). Aerosol samples originating from combustion P sources were found to be more soluble and possibly more bioavailable than those from mineral sources (Anderson et al., 2010).

Atmospheric P has a variety of sources (Fig. 1), including mineral dust, combustion products of natural and anthropogenic origin, agricultural activities (fertilizers and insecticides), bioaerosols, sea-spray and phosphine from freshwater wetlands (Mahowald et al., 2008; Tipping et al., 2014; Wang et al., 2014). The total P (hereafter TP) found in natural waters can be grouped in two major forms (Maher and Woo, 1998): 1) the particulate P (PP) and 2) the dissolved P (DP). The PP mainly originates from mineral material (e.g. hydroxyapatite, brushite, fluoroapatite, variscite, stringite and wavellite) as well as P absorbed to mixed phases (e.g. clay-P, clay-organic-P and metal hydroxide-P). DP on the other hand, includes orthophosphates (i.e. $H_2PO_4^-$, HPO_4^{2-}, PO_4^{3-}; hereafter referred to as PO4), inorganic condensed P (pyro-, meta- and polyphosphates). However, both PP and DP can also contain organic P (OP), of both natural and anthropogenic origin. Naturally emitted OP can be sugar-P, inositol-P, phospholipids, phosphoproteins, phosphoamides mainly associated with plants, animal and bacterial cellular materials (Maher and Woo, 1998) commonly present in atmospheric bioaerosols. In addition, orthophosphate monoesters are known products of ribonucleic acid (RNA) and lipids degradation, that dominate the OP pool in the marine environment, which also contains orthophosphate diesters and phosphonates (Paytan et al., 2003).

Biogeosciences Discuss., doi:10.5194/bg-2016-215, 2016
Manuscript under review for journal Biogeosciences
Published: 8 June 2016

Mineral dust has been estimated to be the largest external to the ocean source of bioavailable P (Okin et al., 2011). Mahowald et al. (2008) estimated a global P mineral source of 1.15 Tg-P yr^{-1}, by taking into account a typical observed P fraction of 720 ppm in dust emissions. Furthermore, they also applied a constant solubility fraction of 10% on the dust mineral source, as observed by Baker et al. (2006) for Saharan P-containing aerosols over the Atlantic ocean, in order to estimate the soluble P source associated with mineral dust. Recently published aerosol and deposition observations of African dust at Miami and Barbados (Zamora et al., 2013) suggest a total P-content of about 880 ppm, which is in the range of P fraction in dust from earlier studies (roughly 700-1090 ppm as reviewed by Mahowald et al. (2008)). Based on OP:OC atomic ratios of 0.001-0.009 observed in several types of soils, Kanakidou et al. (2012) calculated that about 0.03 Tg-P yr^{-1} of OP (10% of which is soluble) is also emitted in the global atmosphere.

P-containing dust solubilisation in deliquesced mineral dust aerosols is expected to significantly contribute to the dissolved inorganic forms of P (DIP) in the atmosphere. Nenes et al. (2011) suggested that dissolution of apatite minerals (i.e. $Ca_5(PO_4)_3(OH,F,Cl)$) under acidic conditions can explain the observed DIP levels over the Eastern Mediterranean, a characteristic region where Saharan dust can interact with polluted air masses from Europe and the Middle East. Under acidic atmospheric conditions, H^+ can react with the PO_4 and the HO- or F- groups in the crystal surface, weakening the Ca^{2+} bonds and thus phosphate is mobilized from the crystal surface (Christoffersen and Christoffersen, 1981). Hence, mineral dust acid dissolution under polluted conditions can potentially release DP in the atmosphere and further stimulate the net primary production of marine ecosystems by increasing the bioavailable P supply into the oceans (Nenes et al. 2011).

Primary P sources from combustion processes of anthropogenic and biomass burning origin are estimated to contribute significantly to global P fluxes in the atmosphere (Mahowald et al., 2008; Wang et al., 2014). However, the estimated strength of the primary P combustion source may vary by about an order of magnitude on the global scale, due to the diversity in the form of the emitted P (i.e. residual or P-containing ash, gaseous or particulate P produced during combustion processes) and in the adopted size distribution of the emitted P-containing particulate matter (e.g. fine or coarse) considered in emission rates calculations (Wang et al., 2014). Mahowald et al. (2008) using observed mass ratios of P to Black Carbon (BC) for fine (mean particle diameter ≤1μm; submicron) and coarse (mean particle diameter > 1μm) particles, calculated emission fluxes from biomass burning and anthropogenic fuel (i.e. fossil fuel and biofuel) combustion of 0.03 Tg-P yr^{-1} and 0.05 Tg-P yr^{-1}, respectively. Wang et al. (2014) taking into account the potential volatilized-P produced during combustion processes, calculated about 30 times higher global atmospheric P emissions from biomass burning and anthropogenic combustion processes (0.7 Tg-P yr^{-1} and 1.8 Tg-P yr^{-1} respectively). Tipping et al. (2014) estimated a global atmospheric P emission flux of 3.7 Tg-P yr^{-1} by combining observed deposition rates over land together with modelled deposition rates over the ocean. This latter emission flux estimate however, also accounts for P deposition fluxes for larger particles that are mainly deposited very close to their source region.

The sea-surface microlayer can also act as an atmospheric source of P in the marine environment (Graham et al., 1979). Correlations between sea-salt fluxes and seawater P concentrations revealed a 10-200 enrichment of P content in sea salt particles compared to sea-water Na concentrations (Graham and Duce, 1979; Graham et al., 1979). However, this enrichment was found to decrease with increasing wind velocity, introducing significant uncertainty to the strength of the oceanic flux of P on a global scale. Mahowald et al. (2008) taking into account a constant Na concentration in seawater of 10.781 g-Na $kg\text{-}water^{-1}$ and surface seawater phosphate concentrations from the NOAA Data Center, calculated a global annual flux of soluble P of 0.005 Tg-P yr^{-1}. Wang et al. (2014), using the median estimate of various experimental and modelling studies (ranging from 0.005-0.33), calculated a mean P-content in sea-salt particles of 6 ppm by weight, which corresponds to a total oceanic emission P flux of 0.16 Tg-P yr^{-1}. Paytan et al. (2003) found that OP in the seawater

Biogeosciences Discuss., doi:10.5194/bg-2016-215, 2016
Manuscript under review for journal Biogeosciences
Published: 8 June 2016

particulate matter can be up to 80% of total P. Based on an observed OP/Na mass ratio of 0.02% by Graham and Duce (1979), Kanakidou et al. (2012) estimated that the surface ocean may also emit 0.19 – 0.80 Tg-P yr^{-1} in the form of OP.

Bioaerosols are P-carriers (Mahowald et al., 2008) that can significantly contribute to the OP budget of the atmosphere (Kanakidou et al., 2012). These primary biological aerosol particles (hereafter PBAPs) usually range from 10 nm to roughly 100 μm in diameter and depending on their sizes, origin and type, can be transported over long distances. PBAPs can be either alive, dead, dormant (e.g. bacteria, viruses and fungi spores) or products released from living organisms such as pollen (Ariya et al., 2009). Mahowald et al. (2008) calculated that PBAP contribute 0.165 Tg-P yr^{-1} while Kanakidou et al. (2012), based on organic carbon (OC) estimates of PBAPs emissions and by using a OP:OC atomic ratio of 0.001, calculated that PBAPs contribute about 0.13 Tg-P yr^{-1} to global OP emissions. Large uncertainties, however, are associated with this estimate since it relies on the applied OP:OC ratios of PBAPs that have been observed to range over 2 orders of magnitude from about 0.0002 up to 0.02 (Kanakidou et al., 2012 and references therein) and on the simplified approximation of the density (1-1.2 g cm^{-3}) used for the conversion of the PBAPs number fluxes to mass units (Burrows et al., 2009a, 2009b). Mahowald et al. (2008) and Kanakidou et al. (2012) assumed half of the PBAP source to be hydrophilic, while Heald and Spracklen (2009) assumed all PBAPs to be totally hydrophilic particles using an OM:OC ratio of 2.6 that is based on observations of fungal spores as proposed by Bauer et al. (2008). However, bacteria (e.g. *P. syringae*) are considered as rather insoluble bioaerosols, in contrast to the water soluble fractions of highly polar sugars (fructose, glucose, sucrose, trehalose) and sugar alcohols (arabitol, inositol, mannitol), mainly contained in pollen grains and fungi spores (Ariya et al., 2009). Ageing during atmospheric transport is also expected to increase bioaerosols solubility, converting a fraction of their insoluble OP content to dissolved OP (DOP) due to the uptake of oxidants and the formation of larger chains of soluble multifunctional groups (Ariya et al., 2009). Recent work also suggests that atmospheric bioaerosol (especially bacteria) are very good CCN, with critical supersaturations below 0.1% (A. Nenes, unpublished work). Regardless of bioaerosols being hydrophilic or not, because they consist of biological material are expected to be bioavailable (Bjórkman and Karl, 1994). The degree of hydrophilicity therefore is more important for determining the relative importance of dry and wet deposition during their supply to the oceans.

In the present study, the 3-D chemical transport global model TM4-ECPL is used to integrate current knowledge on atmospheric P cycle and simulate the atmospheric concentrations and deposition fluxes of P over land and oceans, driven by mineral, natural and combustion P emissions as described in Sect. 2. The effect of atmospheric acidity on the P-mobilization from mineral dust aerosol in atmospheric water, together with the OP atmospheric ageing on the DP global budgets is also presented (Sect. 2). The calculated TP and DP global atmospheric concentrations are presented and compared to observations in Sect. 3. Furthermore, in Sect. 4, the importance of present day air-pollutants on DP atmospheric deposition is investigated based on simulations using past and future anthropogenic and biomass burning emission scenarios. The contribution of bioaerosols to the bioavailable P atmospheric deposition and implications of the findings concerning the biogeochemistry of marine ecosystems are also discussed (Sect. 4). Overall, the impacts of human-driven changes on the calculated DP deposition fluxes to the global ocean are summarized in Sect. 5.

2 Model description

The TM4-ECPL global chemistry – transport model (Myriokefalitakis et al., 2015) simulates the oxidant chemistry accounting for non – methane volatile organics and all major aerosol components, including secondary inorganic aerosols like sulphate (SO_4^{2-}), nitrate (NO_3^-), ammonium (NH_4^+) calculated using ISORROPIA II thermodynamic model (Fountoukis

Biogeosciences Discuss., doi:10.5194/bg-2016-215, 2016
Manuscript under review for journal Biogeosciences
Published: 8 June 2016

and Nenes, 2007) and secondary organic aerosols (Tsigaridis et al., 2014). The atmospheric cycles of Fe and N in TM4-ECPL have been parameterized and evaluated in Myriokefalitakis et al. (2015) and Kanakidou et al. (2016) respectively, while uncertainties in the computed atmospheric composition associated with different emissions parameterizations have been calculated in Daskalakis et al. (2015). The model's ability to reproduce distributions of organic aerosols (Tsigaridis et al., 2014) and tropospheric ozone, ozone's precursors and aerosols have been also evaluated, against satellite and in-situ observations (Quennehen et al., 2015; Eckhardt et al., 2015; Stohl et al., 2015).

TM4-ECPL is driven by meteorology from the ECMWF (European Centre for Medium – Range Weather Forecasts) Interim re–analysis project (ERA – Interim) meteorology (Dee et al., 2011). The current model configuration has a horizontal resolution of 6^o in longitude by 4^o in latitude and 34 hybrid layers in the vertical, from surface up to 0.1 hPa. All simulations have been performed with meteorology for the year 2008 and a model time-step of 30 min. A spin-up time of one year (with 2007 meteorology) has been used. For this study, TM4-ECPL uses anthropogenic (including ships and aircraft emissions) and biomass burning emissions from the historical Atmospheric Chemistry and Climate Model Intercomparison Project (ACCMIP) database (Lamarque et al., 2013) for the year 1850 (hereafter PAST), from the Representative Concentration Pathway 6.0 (RCP 6.0) emission scenario (van Vuuren et al., 2011) for the year 2008 (hereafter PRESENT) and for the year 2100 (hereafter FUTURE) that have been used for the sensitivity simulations. Details on anthropogenic and natural emissions in the model are provided in Myriokefalitakis et al. (2015) with the exception of mineral dust that for the present study is calculated online by the model (van Noije et al., 2014), based on the dust source parameterization of Tegen et al. (2002).

2.1 Phosphorus Emissions

2.1.1 Phosphorus emissions from mineral dust

Apatite is the most abundant primary natural source of P in soils (Newman, 1995) compared to other low solubility P forms such as secondary metal–phosphate precipitates and organic phosphate. For the present study, apatite is assumed to be the only mineral in dust that contains P. The spatially distributed fraction of P in soils (f_P) from the global soil mineralogy dataset developed by Nickovic et al. (2012) is used to calculate the inorganic P-containing mineral (i.e. apatite) emissions as:

$$E_P = F_{880} \cdot f_P \cdot E_{Du} \quad (1)$$

where E_{Du} is the on-line calculated dust emissions in the model, F_{880} is a factor applied to adjust the P emissions to the global mean P content of mineral dust in the model domain of 880 ppm per weight as observed by Zamora et al. (2013), and E_P is the resulted inorganic P emissions from mineral. P-containing minerals associated with dust particles are emitted in the fine and coarse mode with mass median radii (lognormal standard deviation) of 0.34 μm (1.59) and 1.75 μm (2.00), respectively. The apatite emissions from mineral dust calculated for the year 2008 amount to 1.034 Tg-P yr^{-1} with 10% of it (0.103 Tg-P yr^{-1}) in the dissolved form (Table 1).

In addition to the mineral desert dust P source, we account for the OP present in soil's organic matter, following the method presented by Kanakidou et al. (2012 and references therein). Thus, using a mean OP:OC molar ratio of 0.005, a mean OM content of soil dust of 0.25% and an OM:OC molar ratio of 1.76, we here evaluate the dust source of OP at 0.022 Tg-P yr^{-1} for the year 2008. This flux is in good agreement with the 0.03 Tg-P yr^{-1} calculated for 2005 by Kanakidou et al. (2012) using the same methodology but the AEROCOM database for dust emission fluxes (Dentener et al., 2006). Note that similarly to that earlier study, a solubility of 10% is here applied to the OP dust emissions.

Biogeosciences Discuss., doi:10.5194/bg-2016-215, 2016
Manuscript under review for journal Biogeosciences
Published: 8 June 2016

2.1.2 Phosphorus emissions from combustion sources

For the present study, the P/BC mass ratios of combustion sources as estimated by Mahowald et al. (2008) (i.e. 0.0029 for fine aerosols and 0.02 for coarse aerosols) are applied on the inventories of monthly BC emissions of anthropogenic (i.e for fossil fuel, coal, waste and biofuel) and biomass burning origin, as provided by the historical ACCMIP database for 1850 and from the RCP6.0 for 2008 and 2100. The computed anthropogenic combustion and biomass burning annual mean sources of TP are calculated equal to 0.043 Tg-P yr^{-1} and 0.018 Tg-P yr^{-1} respectively, all corresponding to the year 2008. PAST, PRESENT and FUTURE combustion emissions calculated for this study based on the ACCMIP and RCP 6.0 database are presented in Table 1. An additional present-day simulation has been performed taking into account the combustion emissions, as developed by Wang et al. (2014). According to that database, anthropogenic emissions from fossil fuels, biofuels and deforestation fires amount to 1.079 Tg-P yr^{-1} and natural fire emissions equal to 0.808 Tg-P yr^{-1} in the model domain (R. Wang, personal communication, 2016).

For the present study, a number mode radius of 0.04 μm and a lognormal standard deviation of 1.8 are assumed for fine P emissions, while for coarse P a number mode radius of 0.5 μm and lognormal standard deviation of 2.00 are used as proposed for combustion aerosols by Dentener et al. (2006). TP coarse aerosol emissions from anthropogenic combustion are assumed to be 25% of those in the form of fine aerosol emissions (Jacobson and Streets, 2009), while biomass burning coarse emissions are assumed equal to 20% those of fine aerosols (Mahowald et al., 2008). Half of TP emissions from combustion sources are considered to be in the form of OP based on the Kanakidou et al. (2012) recommendations. All P-containing particles from combustion emissions are here treated initially as 50% soluble (Mahowald et al., 2008). The insoluble fraction of OP associated with combustion emissions can be further converted to dissolved OP (DOP) during atmospheric ageing, by assuming the same rate as all primary carbonaceous aerosols in the model (Tsigaridis et al., 2006).

2.1.3 Phosphorus emissions from primary biological aerosol particles

Three types of P-containing PBAPs are considered for the present study: bacteria (hereafter BCT), fungal spores (hereafter FNG) and pollen grains (hereafter PLN). The BCT fluxes are here parameterized based on the Burrows et al. (2009) best-fit estimates for particles of 1 μm diameter flux rates (f) and for six different ecosystems; namely coastal: 900 m^{-2} s^{-1}, crops: 704 m^{-2} s^{-1}, grassland: 648 m^{-2} s^{-1}, land-ice: 7.7 m^{-2} s^{-1}, shrubs: 502 m^{-2} s^{-1} and wetlands: 196 m^{-2} s^{-1}. For the present study, the Olson Global Ecosystem Database (Olson, 1992), originally available for 74 different land types on a spatial scale of 0.5° x 0.5°, is lumped into 10 ecosystem groups as proposed by Burrows et al. (2009). The total BCT flux (F_{BCT}; s^{-1}) in the model is calculated based on the aforementioned fluxes (f_i; m^{-2} s^{-1}) per ecosystem (i), weighted by the respective ecosystem area fraction in the model gridbox (a_i; m^2), as:

$$F_{BTC} = \sum_{i=1}^{6} a_i \cdot f_i \quad (2)$$

Heald and Spracklen (2009) proposed that FNG fluxes linearly depend on the leaf area index (LAI; m^2 m^{-2}) and the specific humidity (q; kg kg^{-1}), based on near-surface mannitol observations. For the present study however, we use a recently published emission parameterization proposed by Hummel et al. (2015), as derived based on fluorescent biological aerosol particles field measurements at various locations across Europe and for spores with a mean diameter of 3μm (eq. 3):

$$F_{FNG} = 20.426 \cdot (T - 275.82K) + 3.93 \cdot 10^4 \cdot q \cdot LAI \quad (3)$$

In the TM4-ECPL that parameterization (eq. 3) is used to calculate FNG emissions online, using monthly averaged LAI distributions and 3-hourly averaged specific humidity (q) and temperature (T) data, as provided by the ERA-Interim.

Biogeosciences Discuss., doi:10.5194/bg-2016-215, 2016
Manuscript under review for journal Biogeosciences
Published: 8 June 2016

PLN emissions maximize when plant surfaces are dry, under high turbulence during the morning hours and during spring months (Jacobson and Streets, 2009). Hoose et al. (2010) parameterised the pollen flux rate as linearly dependent on LAI assuming particles with a mean diameter of 30μm, by simplifying the more sophisticated parameterisation developed by Jacobson and Streets (2009) for a global model. Here, we use the Jacobson and Streets (2009) pollen parameterization (particle mean diameter of 30 μm), with the number pollen flux (F_{PLN}; s^{-1}) to be estimated as:

$$F_{PLN} = f_{PLN} \cdot LAI \cdot R_{month} \cdot R_{hour} \quad (4)$$

where, f_{PLN} = 0.5 $m^{-2}s^{-1}$, the factor R_{month} accounts for the seasonal and R_{hour} the hourly pollen flux variation.

PBAPs are here assumed to be monodisperse spherical particles (Hoose et al., 2010; Hummel et al., 2015) of 1 g cm^{-3} density (Sesartic and Dallafior, 2011) with an organic matter to organic carbon (OM:OC) ratio set equal to 2.6 (that of mannitol) corresponding to a molecular weight equal to 31 g mol^{-1}, as suggested by Heald and Spracklen (2009). According to our model estimates 50.6 Tg-C yr^{-1} are emitted as PBAP. Bacterial emissions are assumed as completely insoluble (Ariya et al., 2009) in emissions, fungal spores are emitted by 50% as soluble aerosols (Mahowald et al., 2008; Kanakidou et al., 2012), while pollen are emitted as totally soluble aerosols (Hoose et al., 2010). A constant mean P:C atomic ratio of 0.001 is used for PBAPs, as suggested by Kanakidou et al. (2012) and all P is assumed in the form of OP. Based on the above parameterizations the model calculates a OP emission flux associated with PBAP equal to 0.195 Tg-P yr^{-1}, of which 0.165 Tg-P yr^{-1} (about 85%) are considered to be in the form of DOP (Table 1). However, because PBAPs consist of biological material they are here considered to be bioavailable, as further discussed in Sect. 4.1 and Sect.4.2. In TM4-ECPL, upon emission the insoluble fraction of PBAPs becomes progressively soluble due to atmospheric ageing. This process that has been seen to occur for instance by degradation of RNA (Paytan et al., 2003), in TM4-ECPL is parameterised with the same rate as all primary organic matter in the model based on oxidant levels as described by Tsigaridis et al. (2006).

2.1.4 Phosphorus emissions from sea-spay

Oceanic P emissions associated with sea-spray are here computed on-line based on a sea-salt emission flux parameterization of Vignati et al. (2010), accounting for fine and coarse modes, with number mode dry radii of 0.09 μm and 0.794 μm, and lognormal standard deviations of 1.59 and 2.00 for accumulation and coarse particles, respectively. The oceanic P emissions in TM4-ECPL are calculated as:

$$E_{PO_4} = \frac{[P]}{[Na]} \cdot E_{Na} \quad (5)$$

where [P] is the P seawater concentrations in μM, [Na] is Na seawater concentration in μM and E_{Na} is the sea-salt emission flux from the ocean surface in kg-Na m^{-2} s^{-1}. In TM4-ECPL, sea-salt particles are emitted from the ocean's surface every time-step using surface wind-speed data from the ERA-Interim database (updated every 3 hours). Surface seawater PO_4 concentrations come from the LEVITUS94 World Ocean Atlas (Conkright et al., 1994; http://iridl.ldeo.columbia.edu/SOURCES/.LEVITUS94/.ANNUAL/.PO4/) ranging up to about 3 μM of PO_4 in the global ocean. Taking into account that the average Na concentration in seawater is about 10.781 g-Na kg-$water^{-1}$ and an average seawater salinity of 35.5 g $kg\text{-}water^{-1}$, the spatial distribution of surface oceanic Na concentrations can be derived from the distribution of the surface salinity concentrations as provided by the LEVITUS94 World Ocean Atlas (Levitus et al., 1994; http://iridl.ldeo.columbia.edu/SOURCES/.LEVITUS94/ .ANNUAL/.sal/). We additionally take into account the OP oceanic emissions, as described in Kanakidou et al. (2012; see supplementary material and referrences therein). For this, the model accounts for a mean seawater OP concentration of 0.2 μM of P, based on Björkman and Karl (2003) observations. Since to

Biogeosciences Discuss., doi:10.5194/bg-2016-215, 2016
Manuscript under review for journal Biogeosciences
Published: 8 June 2016

our knowledge, no spatial distribution of seawater OP concentrations is available, the monthly mean surface chlorophyll a (Chl a) concentrations from MODIS retrievals, used in the model to derive marine primary organic aerosol emissions (Myriokefalitakis et al., 2010), are also used as a proxy to geographically distribute the mean seawater OP concentrations. Overall, the model calculates an emission flux of TP equal to 0.007 Tg-P yr^{-1} from the global ocean (Table 1), from which 0.001 Tg-P yr^{-1} is in the form of OP. Note that for the present study, as for all OP sources, we assume that OP can be transferred to the soluble mode (DOP) due to atmospheric ageing.

2.1.5 Phosphorus emissions from volcanic aerosols

Mahowald et al. (2008) estimated that about 0.006 Tg-P yr^{-1} are associated with volcanic aerosols on a global scale, based on volcanic plume observations. Although a small source of TP on global scale, volcanic ash is found to impact, at least regionally, the ocean nutrients distributions and marine productivity (Henson et al., 2013; Olgun et al., 2013; Uematsu et al., 2004). For the present study, we applied the same global annual mean volcanic flux (see also Table 1), using the distribution of sulphur volcanic emissions by Andres and Kasgnoc (1998). Note that volcanic phosphorus is here assumed to reside in the fine particulate mode and is treated in the model as totally soluble aerosol (i.e. DIP), as proposed by Mahowald et al. (2008). The log-normal size-distribution parameters used for volcanic P aerosol (i.e. a number mode radius of 0.04 μm and a lognormal standard deviation of 1.8) are those proposed by Dentener et al. (2006) for sulphate aerosols from continuous volcanic eruptions.

2.2 Phosphorus acid-mobilization mechanism

Phosphorus mobilization from mineral dust under acidic conditions, is here assumed to occur for the least- and the most-soluble member of apatite minerals as proposed by Nenes et al. (2011); fluorapatite ($Ca_5(PO_4)_3(F)$; hereafter FAP) and hydroxyapatite ($Ca_5(PO_4)_3(OH)$; hereafter HAP), respectively. FAP is considered as a geologically abundant apatite, usually present in the form of igneous or sedimentary carbonate FAP (Guidry and Mackenzie, 2003). However, due to lack of information on the relative abundance and geographic distribution of FAP and HAP in soils, we here assume equal mass fractions of FAP and HAP in apatite containing soils.

The dissolution of FAP and HAP here is treated as a kinetic process, the rate of which depends on the H^+ activity of atmospheric water (i.e. aerosol water and cloud droplets), the reactivity of P species, the ambient temperature and the degree of solution saturation. The phosphate dissolution rate (R), as moles per second of HPO_4^{-2} per gram of apatite, is obtained using the empirical formulation of Lasaga et al. (1994):

$$R = K(T) \cdot a(H^+)^m \cdot f \cdot A \quad (6)$$

where K is the reaction constant in moles m^{-2} s^{-1}, $a(H^+)$ is the H^+ activity, m is the experimentally derived reaction order with respect to the solution H^+ concentration, and A is the specific surface area of each apatite-containing particle in m^2 g^{-1}. The function f (Cama et al., 1999) depends on the solution saturation state ($0 \le f \le 1$) is given by:

$$f = 1 - Q / K_{Eq} \quad (7)$$

where, Q is the reaction activity quotient, K_{Eq} is each apatite equilibrium constant and Q/K_{eq} is the fraction that expresses the state of saturation of the solution (with respect to the apatite), calculated every timestep in the model. Thus, when $f = 1$, the solution is far from equilibrium, therefore the dissolution rate becomes maximum; while as f approaches 0, the solution approaches equilibrium with any remaining undissolved FAP and HAP.

Biogeosciences Discuss., doi:10.5194/bg-2016-215, 2016
Manuscript under review for journal Biogeosciences
Published: 8 June 2016

HAP is experimentally found to be roughly 3 orders of magnitude more soluble than FAP (K_{Eq}(HAP) = $10^{-20.47}$ and K_{Eq}(FAP) = $10^{-23.12}$, as reported by Nenes et al. (2011) based on van Cappellen and Berner (1991). Based on a compilation of experimental determinations of P-dissolution rates of HAP and FAP by Palandri and Kharaka (2004), the dissolution rate of HAP is about an order of magnitude slower than that of FAP under highly acidic conditions (K(HAP) = $10^{-4.29}$ and K(FAP) = $10^{-3.73}$ for pH=0), while under neutral conditions, HAP is found to dissolve two orders of magnitude faster than FAP (K(HAP) = 10^{-6} and K(FAP) = 10^{-8} for pH=7). Moreover, HAP is measured to have almost 8 times larger specific surface area (80.5 m^2 g^{-1}, Bengtsson et al., 2009) compared to that of FAP (10.7 m^2 g^{-1}) which is in agreement with the measured specific surface areas of 8.1-16 m^2 g^{-1} for sedimentary FAP (Guidry and Mackenzie, 2003). Guidry and Mackenzie (2003) have experimentally derived different rate constants (K) for FAP dissolution ranging from 5.75 10^{-6} mol m^{-2} s^{-1} to 6.53 10^{-11} mol m^{-2} s^{-1} with a pH ranging from 2 to 8.5. They further derived the respective reaction orders (*m*) for each pH-region, between 0.01 (for neutral to basic conditions) and 0.81 (for acidic conditions), while the activation energy of the FAP dissolution (E_a) was calculated equal to 8.3 kcal mol^{-1}. For the present study, the dissolution reaction coefficient K for FAP (Table 2), is based on the dissolution experiments by Guidry and Mackenzie (2003), for a range of pH (2-12), temperatures (25–55°C) as well as for various solution saturation states and ionic strengths.

Bengtsson et al. (2009) have experimentally studied the solubility and the surface complexation of non-stoichiometric synthetic HAP, identifying three distinct pH-regions for their batch dissolution experiments: 1) under acidic pH (<4.5) HAP dissolution is relatively high, producing high concentrations of Ca^{2+} and $H_2PO_4^-$; 2) under basic pH (>8.2) surface complexation is the main process and 3) for intermediate pH (4.5-8.2) where both dissolution and surface complexation occur. However, they do not provide sufficient information to enable parameterising HAP dissolution similarly to FAP dissolution. Therefore, for HAP dissolution kinetics we use the dissolution rates of FAP after correcting them to account for the differences between HAP and FAP dissolution kinetics as a function of pH and T, as presented by Palandri and Kharaka (2004). For this, we consider the different dissolution rates for a pH range of 0 to 7-8, which is the range of acidity encountered by atmospheric particles, including dust (e.g. Bougiatioti et al., 2016; Weber et al., 2016). Thus, at the strongly acidic limit (25°C and pH = 0), the dissolution rate of HAP is here assumed to be about 27% (i.e. $10^{-0.56}$ times) slower than that of FAP, but for neutral and basic conditions (and 25°C) HAP dissolves two orders of magnitude faster than FAP (Palandri and Kharaka, 2004). The dissolution rate also changes with temperature; we assume that HAP dissolution has a similar activation energy to FAP (Palandri and Kharaka, 2004; Guidry and Mackenzie, 2003). Additional details for the FAP and HAP mineral dissolution rate parameters are presented in Table 2.

3 Results and Discussion

3.1 Sources of atmospheric phosphorus

Figure 2 presents the annual mean primary TP and DP emissions from the various sources taken into account in the model (in the supplement the emission distribution per source for TP and DP are also presented in Fig. S1 and Fig. S2, respectively). TP emissions (Fig. 2a) maximize over the major deserts of the world (e.g. Sahara, Gobi, Arabian, Kalahari, North American and Australian deserts) with simulated P fluxes up to 100 ng-P m^{-2} s^{-1} (Fig. 2a and Fig. S1a). Secondary maxima of TP emission fluxes of about 0.1-1 ng-P m^{-2} s^{-1} are also calculated over the mid-latitudes of the northern hemisphere (NH), such as China, Europe and the US, due to release to the atmosphere of TP in ash produced during combustion processes of anthropogenic origin (Fig S1b) and over forested areas in equatorial America. Additionally, during

Biogeosciences Discuss., doi:10.5194/bg-2016-215, 2016
Manuscript under review for journal Biogeosciences
Published: 8 June 2016

biomass burning episodes TP is further released to the atmosphere (Fig S1c), however at rates about one order of magnitude lower compared to those of combustion of anthropogenic origin (roughly 0.01 ng-P m^{-2} s^{-1}).

The same pattern (as for TP emissions) is also simulated for the P soluble fraction (Fig. 2b), but with lower emission fluxes (e.g. about 1 ng-P m^{-2} s^{-1} over the Sahara Desert). This is attributed to the solubility of P-containing mineral dust at emission that is the DP present in the desert soil due to weathering. As mentioned in Sect. 2.1.2, this fraction is taken equal to 10% for the present study. Associated mineral DP emissions (Fig. S2a) of 0.106 Tg-P yr^{-1} (as PO4 and/or DOP) are emitted mainly over the Saharan desert region, but significant fluxes are also calculated to occur over other important deserts of the globe. Anthropogenic DP emissions (0.021 Tg P yr^{-1}) occur mainly over densely populated regions of the globe (e.g. the mid-latitudes of the NH; such as China, Europe and the US), with simulated fluxes up to 0.1 ng-P m^{-2} s^{-1} (Fig. S2b). DP emissions from biomass burning contribute about 0.009 Tg-P yr^{-1}, peaking over intense biomass burning areas, e.g. tropical and high latitude forests and showing maxima over Central Africa, Indonesia and Amazonia (Fig. S2c).

The present day annual apatite dissolution flux is calculated equal to 0.119 Tg-P yr^{-1} (Table 3) and shown in Fig 2c. Most of the apatite dissolution fluxes occur downwind of the major dust source regions (i.e. Nigeria downwind the Sahara Desert, Pakistan downwind the Thar Desert and China downwind of the Gobi desert). Over these regions, the long- and regional-range transport of natural and anthropogenic pollutants enhance atmospheric acidity and subsequently P is mobilized from mineral apatite. The model calculates maximum dissolution fluxes downwind the Sahara and Gobi Deserts over the Persian Gulf and the whole Middle East and the Mediterranean basin as well as over the equatorial Atlantic. In addition, enhanced apatite dissolution is calculated over the tropical Atlantic Ocean, India and the outflow of Asia to the Pacific Ocean, in line with observations of changes in solubility during transport of dust across the tropical Atlantic ocean by Baker et al. (2006a).

As explained in Sect. 2, for the present study apatite dissolution flux (Fig. 2c) is due to the respective FAP and HAP solubilisations that occur both in aerosol water and cloud droplets (Fig. S3). The model calculates that most of the apatite dissolution (0.095 Tg-P yr^{-1}) is occurring in deliquesced particles (Fig. 3; S3a and b), mainly attributed to the higher aerosol acidity, with only 0.024 Tg-P yr^{-1} calculated to occur in cloud droplets (Fig. 3b; Fig. S3c and d). Note that in our model, global mean pH in clouds is calculated to be about 4.5 (Myriokefalitakis et al., 2015). However, the distribution of aerosol and cloud dissolution of apatite is rather different, since most of cloud dissolution is calculated to occur i) off-shore the African continent (i.e. over Cote d'Ivoire, Nigeria and Cameroon) over equatorial Atlantic Ocean and ii) over China and India, where dust aerosols downwind of major desert regions (i.e. Sahara and Gobi Desert respectively) meet polluted and acidic cloud droplets.

HAP dissolution flux (Fig. S3d) is calculated to be roughly 60% higher than that of FAP (Fig. S3c) in cloud droplets. The contrary is simulated however for the aerosol dissolution rates (Fig S3a and b), with slightly slower dissolution rate of HAP than FAP due to the saturation factor (*f*) in the aerosol water. Since HAP is more soluble than FAP, the respective mobilized PO4 concentrations increase faster in the aerosol solution and can react with the dissolved Ca^{2+} present in dust, ultimately forming amorphous apatite that precipitates from the solution (i.e. f=1, thus the dissolution process stops). In the presence of dissolved Ca^{2+} and PO4, other salts, such as monenite ($CaHPO_4$) (Somasundaran et al., 1985), can also be formed and further impact the solution's degree of saturation. These results suggest that the solution saturation effect in dust aerosol water can be a critical control on the observed PO4 enhancement in acidic atmosphere conditions.

Finally, a significant amount of DOP (0.037 Tg-P yr^{-1}) is added to the total DP sources due to the ageing of OP-containing aerosols during atmospheric transport (Table 3). This amount corresponds to about 10% of the global DP primary emission sources and to roughly 25% of the total dust-P acid mobilization flux on a global scale. The ageing of OA carrying P presents maxima over forested areas (about 0.1 ng-P m^{-2} s^{-1}) due to the high oxidation of PBAP (Fig. 2d). Secondary maxima

Biogeosciences Discuss., doi:10.5194/bg-2016-215, 2016
Manuscript under review for journal Biogeosciences
Published: 8 June 2016

are also calculated over China (0.01-0.1 ng-P m^{-2} s^{-1}) attributed to ageing of primary OP of anthropogenic origin. Downwind of desert source regions significant DOP production rates, up to 0.1 ng-P m^{-2} s^{-1}, are calculated over the Sahara, the Thar and Gobi Deserts; however these DP formation rates are more localized over continental regions than those due to acid mobilization mechanism of the dust mineral content (Fig. 2c). Non-negligible DOP production is also calculated over the coastal oceans, owing to the OP ageing under the long-range transport in the atmosphere.

3.2 Phosphorus evaluation

Figure 4 presents the model evaluation against P-containing aerosol concentrations and dry deposition fluxes from various locations around the globe. In Fig. 4a the calculated PO4 concentrations in ambient aerosols near the surface are validated against observations by Baker et al. (2010), Martino et al. (2014) and Powell et al. (2015) as well as from Finokalia and Corsica Stations in the eastern and western Mediterranean (Mihalopoulos and co-workers, unpublished data). In Fig. 4b, PO4 deposition fluxes (wet and dry deposition) from the Vet et al. (2014) compilation and from observations at Finokalia Station (Mihalopoulos and co-workers, unpublished data) are also compared with the model derived fluxes for the PRESENT simulation.

Considering the scarcity of observational data and the gaps in knowledge of P emissions and fate in the atmosphere, the computed atmospheric P aerosol concentrations and deposition fluxes satisfactorily compare with available observations with a mean normalized bias (MNB; see definitions of statistical parameters in Myriokefalitakis et al. (2015)) of about -60% for TP (N=609) and PO4 (N=1076) concentrations indicating a model underestimate of the observed values. A slightly larger underestimate (NMB=-64%) is found for the PO4 deposition fluxes (N=547) (Fig. 4b). More detailed comparisons of the model results with observations per database are presented in the supplement. Figures S4a-S4d also compare the results of sensitivity simulations with the observations. These figures indicate an overestimate of TP by the Wang combustion emission database and a reasonable agreement for PO4, while neglecting dissolution of P leads to an underestimate of PO4. Overall, the base case simulation is the one performing the best when accounting both TP and PO4. Figures S5 and S6 present the comparison of the annual cycle of the atmospheric concentrations (TP and PO4) and deposition fluxes (dry and wet deposition), against the TM4-ECPL monthly model results for the PRESENT simulation. For this, all observations, independent of the year, are averaged appropriately (per day or per month) depending on data availability. For cruise measurements over the Atlantic Ocean (Baker et al., 2010; Martino et al., 2014; Powell et al., 2015) and the global compilation of deposition rates (Vet et al., 2014), observations are also spatially averaged inside the same model grid box. Based on these comparisons, we evaluate that an uncertainty of at least an order of magnitude is associated with the model estimates.

3.3 Phosphorus atmospheric concentrations

TM4-ECPL calculates global TP and DP atmospheric burdens of 0.010 Tg-P and of 0.003 Tg-P, respectively. The calculated global annual mean TP and DP atmospheric surface distributions are shown in Fig. 5a and Fig. 5b, respectively. TP surface concentrations maximize over the major dust regions of the world, roughly 0.1-1 μg-P m^{-3} (Fig. 5a), where P-containing dust particles dominate the TP burden. Secondary maxima are calculated over Central Africa, Asia and Indonesia, where significant TP concentrations (10-100 ng-P m^{-3}) are associated with biomass burning emissions and PBAP (Fig. 5a). Over the oceans however, TP concentrations maximize downwind of dust source regions (roughly 10-100 ng-P m^{-3}) and secondary maxima of about 1-10 ng-P m^{-3} are calculated due to long range transport from continental sources, mainly over the NH.

Biogeosciences Discuss., doi:10.5194/bg-2016-215, 2016
Manuscript under review for journal Biogeosciences
Published: 8 June 2016

Maxima annual mean DP concentrations of 100 ng-P m^{-3} are calculated to occur over the Sahara, the Arabian and the Gobi deserts near the surface (Fig. 5b). The outflow from these source regions transports DP over the global ocean with annual mean concentrations of about 10 ng-P m^{-3} downwind dust source regions, with the highest impact calculated for the tropical Atlantic Ocean. The simulated concentrations of DP over polluted regions range from 1 to 10 ng-P m^{-3}, further highlight the importance of anthropogenic contributions to the DP atmospheric burden - directly due to combustion emissions and indirectly due to the mobilization of P when atmospheric transport of dust co-exists with atmospheric pollution (Fig. 5b). TP emissions associated with African dust are calculated to significantly affect the lower troposphere (Fig. 5c). Furthermore, DP shows non negligible concentrations (Fig. 5d) in the middle troposphere that are attributed to transport from the source regions and to atmospheric ageing (mainly P-mobilization processes) that convert insoluble to dissolved P, as already discussed.

3.4 Present day phosphorus deposition flux

TM4-ECPL calculates that 1.314 Tg-P yr^{-1} of TP are deposited to the Earth's surface of which about 0.265 Tg-P yr^{-1} over the ocean (Table 4), which is almost 2 times lower than that estimated by Mahowald et al. (2008) (0.558 Tg-P yr^{-1}) but at the low end of the deposition flux range calculated by Wang et al. (2014) (0.9-7.8 Tg-P yr^{-1} over the globe with 0.2-1.6 Tg-P yr^{-1} over the ocean). The highest TP annual deposition fluxes (up to 100 ng-P m^{-2} s^{-1}) are calculated to occur over the Sahara and Gobi deserts while deposition fluxes up to 1 ng-P m^{-2} s^{-1} are also calculated at the outflow from dust source regions, especially over the Equatorial Atlantic and Northern Pacific Oceans (Fig. 6a). The computed global DP deposition is calculated equal to 0.423 Tg-P yr^{-1}, of which 0.156 Tg-P yr^{-1} is deposited over the ocean (Table 4), which is about 60% higher than the estimate by Mahowald et al. (2008) (0.096 Tg-P yr^{-1}). The highest DP deposition fluxes are also simulated to occur downwind of dust source regions, owing to the DP content of the primary P emissions discussed in Sect. 3.1, as well as due to P-solubilisation by aerosol ageing during atmospheric transport (Fig. 6b). Secondary DP deposition flux maxima (about 0.1 ng-P m^{-2} s^{-1}) are simulated downwind of highly forested regions (i.e. Amazonia, Central Africa and Indonesia), mainly due to the contribution of PBAPs to the DOP concentrations in the atmosphere.

Figure S7 further presents the seasonal variability of DP deposition fluxes as calculated by TM4-ECPL. The maximum seasonal DP deposition flux over the ocean of 0.045 Tg-P is calculated to occur during June-July-August (Fig. S7c), followed by 0.043 Tg-P during March-April-May (Fig. S7b) and by 0.036 Tg-P during September- October-November (Fig. S7d). The maximum DP deposition flux in summer occurs when ocean stratification maximizes thus leading to the highest impact of atmospheric deposition to the marine ecosystems (Christodoulaki et al., 2013). Furthermore, PBAP contribution maximizes in summer at regions with important biogenic emissions (Figure S8e-h), while dust contribution maximizes in spring mainly over and downwind the major deserts in the tropical and mid-latitudes of the northern hemisphere (Figure S8a-d). The enhanced photochemistry during NH spring and summer increases atmospheric oxidants and the atmospheric acidity due to NO_x and SO_x oxidation. Note also that under equinox conditions, in particular in spring, Sahara dust outbreaks are also favored (Fig. S8b). Considering that most TP emissions occur in the NH (Fig. 2a), DP secondary formation from IP and OP source is simulated to maximizing there (Fig. 2c,d), with emissions from biomass burning and combustion of anthropogenic origin to further contribute to the DP deposition flux.

3.5 Phosphorus solubility

The present-day P solubility of deposited aerosols (hereafter SP = %DP/TP) is calculated to vary spatially significantly (Fig. 7a), with minima (as low as 10%) over dust sources like the Sahara (where the insoluble fraction of TP dominates aerosol

Biogeosciences Discuss., doi:10.5194/bg-2016-215, 2016
Manuscript under review for journal Biogeosciences
Published: 8 June 2016

content) and maxima (more than 90%) over remote oceanic regions such as the equatorial Pacific, the southern Atlantic, the Indian and the Southern Oceans (where DP is associated with more aged aerosols). The individual contributions of each source to the atmospheric SP are shown in Fig. S9 (i.e. within each model grid these fractions sum up to 100%).

The low SP values over dust source regions are mainly attributed to the relatively low both weathering of dust aerosols (10%) assumed in emission fluxes and mineral P-dissolution rate (Fig. S9a). The low water associated with dust aerosols near dust sources and to the enhanced buffering capacity by dust carbonate leading to excess of Ca^{2+} concentrations) (see Sect. 3.1 and Fig. 2c) are thus causing low P dissolution. The model calculates high SP values (up to 50-60%) over regions such as the Mediterranean basin, where the co-existence of relatively high dust concentrations and high amounts of anthropogenic pollutants (e.g. Kanakidou et al., 2011) tends to enhance significantly atmospheric processing of mineral P (Nenes et al., 2011). High dust SP values are also calculated over the open ocean of the NH, the Atlantic Ocean, the Pacific Ocean in the outflow of the America, downwind of the Arabian Desert over the Indian Ocean and over the European continent. These results are attributed to the mineral P-mobilization under polluted acidic atmospheric conditions.

Anthropogenic combustion aerosols are calculated to contribute significantly to SP (20%-30%) over highly populated regions of the word, mainly over the NH as in the case of the eastern and the western coasts of the US, central and Northern Europe and Western Asia (Fig. S9b). About 5-15% of the calculated SP over the remote oceans is attributed to long range transport during which aerosols have been subject to atmospheric ageing. Biomass burning aerosols are calculated to contribute regionally less than 30% to SP, with their maximum contribution over the equatorial Atlantic and Indian Oceans due to aerosol transport and the atmospheric ageing from Central Africa and India (Fig. S9c). DP emissions and atmospheric ageing associated with PBAPs from terrestrial sources are calculated to significantly contribute to DP deposition in the tropics; about 50% in the outflow of Amazonia and Central African and Indonesian forests on annual mean basis (Fig. S9d). Seasonally, this contribution is even higher, for instance it reaches 60% in the Mediterranean during summer and 70% in the outflow over the equatorial Pacific Ocean (not shown). DP from sea-spay dominates over all the remote Southern Ocean where no other significant primary source of DP is present (Fig. S9e), while volcanic eruptions contribute to the SP mainly over the equatorial and Northern Pacific Ocean (Fig. S9f).

4 Sensitivity of dissolved phosphorus budget to air-pollutants

Atmospheric acidity strongly depends on SO_x, NO_x and NH_x anthropogenic emissions and impacts on dust solubility. It is thus expected to change following the variability in the anthropogenic emissions of air pollutants (Weber et al., 2016). The response of atmospheric ageing of TP, which converts the insoluble TP fraction partially to DP, to air pollutant emission changes is here assessed by comparing simulations performed using anthropogenic and biomass burning past and future emissions to the present-day simulation (see Sect. 2). In addition to apatite dissolution changes, atmospheric OA ageing is also affected by changes in oxidants levels (Tsigaridis et al., 2006). Furthermore, primary anthropogenic and biomass burning emissions of P also vary, as shown in Table 1 and discussed in Sect. 2.1. In particular, TP anthropogenic emissions are estimated to have increased by a factor of 5.5 since PAST and to be reduced back to the PAST levels in the FUTURE. In the simulations discussed here, meteorology and natural emissions of dust, sea-salt, PBAP and from volcanoes are kept constant; to those of the year 2008 (i.e. PRESENT simulation). Hence, the computed changes for species that regulate the mineral-P acid mobilization (e.g. SO_4^{2-}, NO_3^-, NH_4^+) are due to the respective combustion emission differences between PAST, PRESENT and FUTURE simulations. For the PAST simulation, the anthropogenic emissions (e.g. NO_x, NH_x and SO_x) are a factor of 5-10 lower than present day emissions (Lamarque et al., 2013). Compared to the present day, the model

Biogeosciences Discuss., doi:10.5194/bg-2016-215, 2016
Manuscript under review for journal Biogeosciences
Published: 8 June 2016

calculates significant changes in the aerosol-pH in the past simulation with less acidic pH near the surface of the NH oceans, but a more acidic pH over the US due to extensive coal combustion in 1850 (Myriokefalitakis et al., 2015). The FUTURE simulation projects globally a less acidic aerosol pH than present day (Myriokefalitakis et al., 2015), owing to lower NO_x and SO_x emissions. Indeed, for the future simulation, anthropogenic emissions (RCP6.0) for most of the continental areas are projected to be lower than the present-day and to almost return to pre-1980 levels due to air quality regulations (Lamarque et al., 2013). However, as discussed in Myriokefalitakis et al. (2015) for the atmospheric cycle of Fe, because biomass burning emissions are projected to increase in the future the system does not fully return to pre-1980 conditions. Past and future changes of the atmospheric acidity have a significant effect on mineral-P dissolution (Fig. S10c,d) and on the ageing of atmospheric OP (Fig. S10e,f). For the PAST simulation the model calculates about 43% lower acid mineral-P dissolution (0.068 Tg-P yr^{-1}) compared to present-day (0.119 Tg-P yr^{-1}) while the FUTURE acid mineral-P mobilization flux (0.084 Tg-P yr^{-1}) is also projected almost 30% lower than nowadays (Table 3).

4.1 Past and future changes in the phosphorus deposition flux

The global annual deposition fluxes of TP and DP as computed by TM4-ECPL for the three main simulations (PAST, PRESENT, FUTURE) are provided in Table 4. In addition in the same Table, the sum of the DP and the insoluble PBAP deposition, which is considered being bioavailable since it is biological material, is reported as bioavailable P (BP). For the PAST simulation, the model calculates a global TP deposition flux (Table 4) that is about 3% lower than the present-day flux. Significant increases in TP deposition fluxes since the PAST have been calculated over Indonesia and South-eastern Asia (Fig. 6c), as a result of the present high anthropogenic emissions over China. As for the FUTURE simulation, TP deposition is projected to decrease globally by 2.5% compared to present-day (Table 4) with a maximum decrease (up to 40%) due to emission control measures calculated for Europe, the Eastern US and China.

On global scale DP deposition fluxes are also calculated to be lower by about 17% for the PAST and by about 12% for the FUTURE simulations compared to the PRESENT one (Table 4). Although on global scale these reductions are computed to be relatively low, regional reductions can be stronger (up to 60%, Fig. 6d), especially over highly populated regions (e.g. China, Europe) and downwind of major dust sources (e.g. India and Western US). Indeed, present-day DP emission fluxes from anthropogenic combustion (0.021 Tg-P yr^{-1}) are calculated to decrease by about 80% on a global scale both for the PAST and FUTURE simulations (Table 1). According to our calculations, however, present-day DP biomass burning emissions have increased by about 28% from PAST and are expected to further increase by about 22% in the FUTURE. When accounting for both DP anthropogenic combustion and biomass burning emissions, a 2.7 times increase is computed from the PAST to PRESENT and a decrease to half is expected for the FUTURE, contributing significantly to the DP atmospheric deposition changes. Hence, DP deposition fluxes are projected to decrease over the mid-latitudes of the NH where human activities dominate (Fig. 6f), with the largest changes up to 60% over China due to the expected air-quality measures, while smaller changes are computed over India due to the expected increase in its population. Note that our simulations neglect any change in the PBAPs emissions that has occurred in the past or is expected to take place in the future. Therefore, the changes in BP deposition fluxes shown in Table 4 are driven by changes in the anthropogenic and biomass burning emissions and in the atmospheric oxidants that enhance P dissolution during atmospheric ageing.

4.2 Biogeochemical implications of changes in bioavailable phosphorus deposition

Dust contribution to BP deposition to the ocean maximizes over the ocean in the outflow from desert regions mainly in the north hemisphere tropics and mid latitudes (Fig. 7b). However, according to our simulations DOP is an important fraction of

Biogeosciences Discuss., doi:10.5194/bg-2016-215, 2016
Manuscript under review for journal Biogeosciences
Published: 8 June 2016

BP, mainly over continental regions. It is remarkable that bioaerosols are found to be the major contributors to the DP (about 52%) and the BP (about 57%) deposition fluxes on a global scale, which shows that biological material is a major atmospheric carrier of bioavailable P to the ocean (Fig. 7c). This finding implies a potentially important impact of the terrestrial to the marine ecosystems. Our results also indicate that primary anthropogenic emissions of DP as well as anthropogenically driven atmospheric acidity increased the DP supply to the global ocean since the preindustrial period thus providing an important external to the ocean source of nutrients for the marine ecosystem. These results may be particularly important for ecosystems like the East Mediterranean where phytoplankton growth is limited by P availability.

It is also noteworthy that the bioavailable P deposition flux maximizes in summer when ocean stratification is also the strongest, thus leading to the highest impact of atmospheric deposition to the marine ecosystems (Christodoulaki et al., 2013). This flux needs to be taken into account to evaluate the atmospheric DP deposition impact on marine ecosystems. The computed atmospheric deposition of BP over the global ocean of 0.16 Tg-P yr^{-1} represents about 15 % of the global riverine flux to the ocean of 0.99 Tg-P yr^{-1} (Meybeck, 1982). However, while riverine inputs affect mainly the coastal regions, atmospheric deposition is a source of nutrients for the open sea (e.g. Okin et al., 2011).

5 Conclusions

Primary TP and DP emissions together with the atmospheric processing of P are taken into account in the state-of-the-art atmospheric chemistry transport global model TM4-ECPL. Accounting for DP (both inorganic and organic) primary source of 0.314 Tg-P yr^{-1} together with a PO4 acid-mobilization flux of 0.119 Tg-P yr^{-1} and a DOP ageing flux of 0.037 Tg-P yr^{-1}, result overall in a present-day atmospheric DP burden of 0.003 Tg-P and a global DP annual deposition flux of 0.433 Tg-P yr^{-1}, of which 0.156 Tg-P yr^{-1} is deposited over the oceans. P solubility in deposited aerosols is calculated to vary spatially with minima over the dust sources (<10%) and maxima over the remote ocean (up to 90%).

Sensitivity simulations show that increases in anthropogenic and biomass burning emissions since preindustrial times resulted in both enhanced DP combustion primary emissions and P-dissolution occurring under a more acidic environment. Air-quality regulations however, are projected to decrease anthropogenic emissions, mitigate oxidant levels and limit future atmospheric acidity. Focusing on oceanic regions, the last 150 years atmospheric composition change is calculated to have increased the DP deposition to the ocean by about 25% (i.e. 0.123 Tg-P yr^{-1} in preindustrial times against 0.156 Tg-P yr^{-1} nowadays). Projection based on future combustion emissions, drives the model to a 30% reduction in mineral P dissolution flux (0.084 Tg-P yr^{-1} in the future compared to 0.119 Tg-P yr^{-1} in the present day) and taking into account an 80% reduction of the anthropogenic DP emissions, the model calculates an oceanic DP deposition flux of 0.134 Tg-P yr^{-1} that is about 16% lower than present-day. Our results further indicate a significant contribution to the calculated DP deposition fluxes of DIP up to 90%, over the Northern tropical Atlantic, Pacific and Southern Oceans, as well as a DOP contribution higher than 50% over the equatorial oceanic regions.

The contribution of PBAPs deposition to the total bioavailable P to the marine environment is found to exceed 50%, indicating the existence of potential important interactions between the terrestrial and the marine biosphere. Therefore, our results provide new insights to the atmospheric P cycle by demonstrating that PBAPs are as important carriers of bioavailable P as dust aerosol, that was up to now considered as the only large source of DP external to the open ocean.

Although the present global modelling study is based on the current understanding of the processes that drive the atmospheric cycle of P, comparison of model results to observations showed that the model underestimates the data by roughly 50%. Improvements, thus, require reduction in the large uncertainties that still exist with regard to the primary TP

and DP emissions from anthropogenic and natural sources and the adopted kinetic parameters of mineral-P dissolution and organic aerosol-P ageing and their response to the changes in atmospheric acidity. Finally, in view of the importance of P as a nutrient for marine and terrestrial ecosystems in terms of carbon storage and nitrogen fixation, the calculated changes in P deposition due to projected air-quality changes, indicate the necessity to account for feedbacks between atmospheric chemistry, climate and biogeochemical cycles.

Acknowledgements. This research has been co-financed by the European Union (European Social Fund – ESF) and Greek national funds through the Operational Program "Education and Lifelong Learning" of the National Strategic Reference Framework (NSRF) - Research Funding Program: ARISTEIA – PANOPLY (Pollution Alters Natural Aerosol Composition: implications for Ocean Productivity, cLimate and air qualitY) grant. SM acknowledges the European FP7 collaborative project BACCHUS (Impact of Biogenic versus Anthropogenic emissions on Clouds and Climate: towards a Holistic UnderStanding) for financial support. The authors thank Dr. T. van Noije for dust emission module availability, Dr. R. Wang for providing anthropogenic and natural combustion P emission data, P. Nicolaou, A. Mitsotaki, Dr. C. Theodosi, Dr. P. Zarbas and Dr. G. Kouvarakis for the observations in the Mediterranean and Dr. R. Vet for providing P deposition data.

References

Anderson, L. D., Faul, K. L. and Paytan, A.: Phosphorus associations in aerosols: What can they tell us about P bioavailability?, Mar. Chem., 120(1-4), 44–56, doi:10.1016/j.marchem.2009.04.008, 2010.

Andres, R. J. and Kasgnoc, A. D.: A time-averaged inventory of subaerial volcanic sulfur emissions, J. Geophys. Res., 103(D19), 25251, doi:10.1029/98JD02091, 1998.

Ariya, P. A., Sun, J., Eltouny, N. A., Hudson, E. D., Hayes, C. T. and Kos, G.: Physical and chemical characterization of bioaerosols – Implications for nucleation processes, Int. Rev. Phys. Chem., 28(1), 1–32, doi:10.1080/01442350802597438, 2009.

Baker, A. R., French, M. and Linge, K. L.: Trends in aerosol nutrient solubility along a west–east transect of the Saharan dust plume, Geophys. Res. Lett., 33(7), L07805, doi:10.1029/2005GL024764, 2006a.

Baker, A. R., Jickells, T. D., Witt, M. and Linge, K. L.: Trends in the solubility of iron, aluminium, manganese and phosphorus in aerosol collected over the Atlantic Ocean, Mar. Chem., 98(1), 43–58, doi:10.1016/j.marchem.2005.06.004, 2006b.

Baker, A. R., Lesworth, T., Adams, C., Jickells, T. D. and Ganzeveld, L.: Estimation of atmospheric nutrient inputs to the Atlantic Ocean from 50°N to 50°S based on large-scale field sampling: Fixed nitrogen and dry deposition of phosphorus, Global Biogeochem. Cycles, 24(3), doi:10.1029/2009GB003634, 2010.

Bauer, H., Schueller, E., Weinke, G., Berger, A., Hitzenberger, R., Marr, I. L. and Puxbaum, H.: Significant contributions of fungal spores to the organic carbon and to the aerosol mass balance of the urban atmospheric aerosol, Atmos. Environ., 42(22), 5542–5549, doi:10.1016/j.atmosenv.2008.03.019, 2008.

Bengtsson, Å., Lindegren, M., Sjöberg, S. and Persson, P.: Dissolution, adsorption and phase transformation in the fluorapatite–goethite system, Appl. Geochemistry, 22(9), 2016–2028, doi:10.1016/j.apgeochem.2007.05.001, 2007.

Bengtsson, Å., Shchukarev, A., Persson, P. and Sjöberg, S.: A solubility and surface complexation study of a non-stoichiometric hydroxyapatite, Geochim. Cosmochim. Acta, 73(2), 257–267, doi:10.1016/j.gca.2008.09.034, 2009.

Benitez-Nelson, C. R.: The biogeochemical cycling of phosphorus in marine systems, Earth-Science Rev., 51(1-4), 109–135, doi:10.1016/S0012-8252(00)00018-0, 2000.

Björkman, K. and Karl, D.: Bioavailability of inorganic and organic phosphorus compounds to natural assemblages of microorganisms m Hawaiian coastal waters, Mar. Ecol. Prog. Ser., 111(3), 265–273, doi:10.3354/meps111265, 1994.

Björkman, K. M. and Karl, D. M.: Bioavailability of dissolved organic phosphorus in the euphotic zone at Station ALOHA, North Pacific Subtropical Gyre, Limnol. Oceanogr., 48(3), 1049–1057, doi:10.4319/lo.2003.48.3.1049, 2003.

Bougiatioti, A., Nikolaou, P., Stavroulas, I., Kouvarakis, G., Weber, R., Nenes, A., Kanakidou, M. and Mihalopoulos, N.: Particle water and pH in the eastern Mediterranean: source variability and implications for nutrient availability, Atmos. Chem. Phys., 16(7), 4579–4591, doi:10.5194/acp-16-4579-2016, 2016.

Burrows, S. M., Butler, T., Jöckel, P., Tost, H., Kerkweg, A., Pöschl, U. and Lawrence, M. G.: Bacteria in the global atmosphere – Part 2: Modeling of emissions and transport between different ecosystems, Atmos. Chem. Phys., 9(23), 9281–9297, doi:10.5194/acp-9-9281-2009, 2009a.

Burrows, S. M., Elbert, W., Lawrence, M. G. and Pöschl, U.: Bacteria in the global atmosphere – Part 1: Review and synthesis of literature data for different ecosystems, Atmos. Chem. Phys., 9(23), 9263–9280, doi:10.5194/acp-9-9263-2009, 2009b.

Cama, J., Ayora, C. and Lasaga, A. C.: The deviation-from-equilibrium effect on dissolution rate and on apparent variations in activation energy, Geochim. Cosmochim. Acta, 63(17), 2481–2486, doi:10.1016/S0016-7037(99)00144-1, 1999.

van Cappellen, P. and Berner, R. A.: Fluorapatite crystal growth from modified seawater solutions, Geochim. Cosmochim. Acta, 55(5), 1219–1234, doi:10.1016/0016-7037(91)90302-L, 1991.

Christodoulaki, S., Petihakis, G., Kanakidou, M., Mihalopoulos, N., Tsiaras, K. and Triantafyllou, G.: Atmospheric deposition in the Eastern Mediterranean. A driving force for ecosystem dynamics, J. Mar. Syst., 109-110, 78–93, doi:10.1016/j.jmarsys.2012.07.007, 2013.

Christoffersen, J. and Christoffersen, M. R.: Kinetics of dissolution of calcium hydroxyapatite, J. Cryst. Growth, 53(1), 42–54, doi:10.1016/0022-0248(81)90054-3, 1981.

Conkright, M. E., Boyer, T. P. and Levitus, S.: World Ocean Atlas: 1994 Nutrients., 1994.

Cook, A. M., Daughton, C. G. and Alexander, M.: Phosphorus-containing pesticide breakdown products: quantitative utilization as phosphorus sources by bacteria., Appl. Environ. Microbiol., 36(5), 668–72, 1978.

Daskalakis, N., Myriokefalitakis, S. and Kanakidou, M.: Sensitivity of tropospheric loads and lifetimes of short lived pollutants to fire emissions, Atmos. Chem. Phys., 15(6), 3543–3563, doi:10.5194/acp-15-3543-2015, 2015.

Dee, D. P., Uppala, S. M., Simmons, A. J., Berrisford, P., Poli, P., Kobayashi, S., Andrae, U., Balmaseda, M. A., Balsamo, G., Bauer, P., Bechtold, P., Beljaars, A. C. M., van de Berg, L., Bidlot, J., Bormann, N., Delsol, C., Dragani, R., Fuentes, M., Geer, A. J., Haimberger, L., Healy, S. B., Hersbach, H., Hólm, E. V, Isaksen, L., Kållberg, P., Köhler, M., Matricardi, M., McNally, A. P., Monge-Sanz, B. M., Morcrette, J.-J., Park, B.-K., Peubey, C., de Rosnay, P., Tavolato, C., Thépaut, J.-N. and Vitart, F.: The ERA-Interim reanalysis: configuration and performance of the data assimilation system, Q. J. R. Meteorol. Soc., 137(656), 553–597, doi:10.1002/qj.828, 2011.

Dentener, F., Kinne, S., Bond, T., Boucher, O., Cofala, J., Generoso, S., Ginoux, P., Gong, S., Hoelzemann, J. J., Ito, A., Marelli, L., Penner, J. E., Putaud, J.-P., Textor, C., Schulz, M., van der Werf, G. R. and Wilson, J.: Emissions of primary aerosol and precursor gases in the years 2000 and 1750 prescribed data-sets for AeroCom, Atmos. Chem. Phys., 6(12), 4321–4344, doi:10.5194/acp-6-4321-2006, 2006.

Deutsch, C., Sarmiento, J. L., Sigman, D. M., Gruber, N. and Dunne, J. P.: Spatial coupling of nitrogen inputs and losses in the ocean., Nature, 445(7124), 163–7, doi:10.1038/nature05392, 2007.

Duce, R., LaRoche, J., Altieri, K., Arrigo, K. R., Baker, A. ., Capone, D. G., Cornell, S., Dentener, F., Galloway, J., Ganeshram, R. S., Geider, R. J., Jickells, T., Kuypers, M. M., Langlois, R., Liss, P. S., Liu, S. M., Middelburg, J. J., Moore, C. M., Nickovic, S., Oschlies, A., Pedersen, T., Prospero, J., Schlitzer, R., Seitzinger, S., Sorensen, L. L., Uematsu, M., Ulloa, O., Voss, M., Ward, B. and Zamora, L.: Impacts of atmospheric anthropogenic nitrogen on the open ocean., Science, 320(5878), 893–7, doi:10.1126/science.1150369, 2008.

Eckhardt, S., Quennehen, B., Olivié, D. J. L., Berntsen, T. K., Cherian, R., Christensen, J. H., Collins, W., Crepinsek, S., Daskalakis, N., Flanner, M., Herber, A., Heyes, C., Hodnebrog, Ø., Huang, L., Kanakidou, M., Klimont, Z., Langner, J., Law, K. S., Lund, M. T., Mahmood, R., Massling, A., Myriokefalitakis, S., Nielsen, I. E., Nøjgaard, J. K., Quaas, J., Quinn, P. K., Raut, J.-C., Rumbold, S. T., Schulz, M., Sharma, S., Skeie, R. B., Skov, H., Uttal, T., von Salzen, K. and Stohl, A.: Current model capabilities for simulating black carbon and sulfate concentrations in the Arctic atmosphere: a multi-model evaluation using a comprehensive measurement data set, Atmos. Chem. Phys., 15(16), 9413–9433, doi:10.5194/acp-15-9413-2015, 2015.

Elser, J. J., Bracken, M. E. S., Cleland, E. E., Gruner, D. S., Harpole, W. S., Hillebrand, H., Ngai, J. T., Seabloom, E. W., Shurin, J. B. and Smith, J. E.: Global analysis of nitrogen and phosphorus limitation of primary producers in freshwater, marine and terrestrial ecosystems, Ecol. Lett., 10(12), 1135–1142, doi:10.1111/j.1461-0248.2007.01113.x, 2007.

Fountoukis, C. and Nenes, A.: ISORROPIA II: a computationally efficient thermodynamic equilibrium model for K^+ - Ca^{+2} – Mg^{+2} – NH_4^+ – Na^+ – SO_4^{-2} – NO_3^-, Atmos. Chem. Phys., 7(17), 4639–4659, doi:10.5194/acp-7-4639-2007, 2007.

Graham, W. F. and Duce, R. A.: Atmospheric pathways of the phosphorus cycle, Geochim. Cosmochim. Acta, 43(8), 1195–1208, doi:10.1016/0016-7037(79)90112-1, 1979.

Graham, W. F., Piotrowicz, S. R. and Duce, R. A.: The sea as a source of atmospheric phosphorus, Mar. Chem., 7(4), 325–342, doi:10.1016/0304-4203(79)90019-7, 1979.

Guidry, M. W. and Mackenzie, F. T.: Experimental study of igneous and sedimentary apatite dissolution, Geochim. Cosmochim. Acta, 67(16), 2949–2963, doi:10.1016/S0016-7037(03)00265-5, 2003.

Heald, C. L. and Spracklen, D. V.: Atmospheric budget of primary biological aerosol particles from fungal spores, Geophys. Res. Lett., 36(9), L09806, doi:10.1029/2009GL037493, 2009.

Henson, S. A., Painter, S. C., Penny Holliday, N., Stinchcombe, M. C. and Giering, S. L. C.: Unusual subpolar North Atlantic phytoplankton bloom in 2010: Volcanic fertilization or North Atlantic Oscillation?, J. Geophys. Res. Ocean., 118(10), 4771–4780, doi:10.1002/jgrc.20363, 2013.

Hoose, C., Kristjánsson, J. E. and Burrows, S. M.: How important is biological ice nucleation in clouds on a global scale?, Environ. Res. Lett., 5(2), 024009, doi:10.1088/1748-9326/5/2/024009, 2010.

Hummel, M., Hoose, C., Gallagher, M., Healy, D. a., Huffman, J. A., O'Connor, D., Pöschl, U., Pöhlker, C., Robinson, N. H., Schnaiter, M., Sodeau, J. R., Stengel, M., Toprak, E. and Vogel, H.: Regional-scale simulations of fungal spore aerosols using an emission parameterization adapted to local measurements of fluorescent biological aerosol particles, Atmos. Chem. Phys., 15(11), 6127–6146, doi:10.5194/acp-15-6127-2015, 2015.

Jacobson, M. Z. and Streets, D. G.: Influence of future anthropogenic emissions on climate, natural emissions, and air quality, J. Geophys. Res., 114(D8), D08118, doi:10.1029/2008JD011476, 2009.

Jickells, T. D., An, Z. S., Andersen, K. K., Baker, A. R., Bergametti, G., Brooks, N., Cao, J. J., Boyd, P. W., Duce, R. A., Hunter, K. A., Kawahata, H., Kubilay, N., laRoche, J., Liss, P. S., Mahowald, N., Prospero, J. M., Ridgwell, A. J., Tegen, I. and Torres, R.: Global Iron Connections Between Desert Dust, Ocean Biogeochemistry, and Climate, Science (80-.)., 308(5718), 67–71, doi:10.1126/science.1105959, 2005.

Kanakidou, M., Duce, R. A., Prospero, J. M., Baker, A. R., Benitez-Nelson, C., Dentener, F. J., Hunter, K. A., Liss, P. S., Mahowald, N., Okin, G. S., Sarin, M., Tsigaridis, K., Uematsu, M., Zamora, L. M. and Zhu, T.: Atmospheric fluxes of organic N and P to the global ocean, Global Biogeochem. Cycles, 26(3), doi:10.1029/2011GB004277, 2012.

Kanakidou, M., Mihalopoulos, N., Kindap, T., Im, U., Vrekoussis, M., Gerasopoulos, E., Dermitzaki, E., Unal, A., Koçak, M., Markakis, K., Melas, D., Kouvarakis, G., Youssef, A. F., Richter, A., Hatzianastassiou, N., Hilboll, A., Ebojie, F., Wittrock, F., von Savigny, C., Burrows, J. P., Ladstaetter-Weissenmayer, A. and Moubasher, H.: Megacities as hot spots of air pollution in the East Mediterranean, Atmos. Environ., 45(6), 1223–1235, doi:10.1016/j.atmosenv.2010.11.048, 2011.

Kanakidou, M., Myriokefalitakis, S., Daskalakis, N., Fanourgakis, G., Nenes, A., Baker, A. R., Tsigaridis, K. and Mihalopoulos, N.: Past, Present, and Future Atmospheric Nitrogen Deposition, J. Atmos. Sci., 73(5), 2039–2047, doi:10.1175/JAS-D-15-0278.1, 2016.

Lamarque, J.-F., Shindell, D. T., Josse, B., Young, P. J., Cionni, I., Eyring, V., Bergmann, D., Cameron-Smith, P., Collins, W. J., Doherty, R., Dalsoren, S., Faluvegi, G., Folberth, G., Ghan, S. J., Horowitz, L. W., Lee, Y. H., MacKenzie, I. A., Nagashima, T., Naik, V., Plummer, D., Righi, M., Rumbold, S. T., Schulz, M., Skeie, R. B., Stevenson, D. S., Strode, S., Sudo, K., Szopa, S., Voulgarakis, A. and Zeng, G.: The Atmospheric Chemistry and Climate Model Intercomparison Project (ACCMIP): overview and description of models, simulations and climate diagnostics, Geosci. Model Dev., 6(1), 179–206, doi:10.5194/gmd-6-179-2013, 2013.

Lasaga, A. C., Soler, J. M., Ganor, J., Burch, T. E. and Nagy, K. L.: Chemical weathering rate laws and global geochemical cycles, Geochim. Cosmochim. Acta, 58(10), 2361–2386, doi:10.1016/0016-7037(94)90016-7, 1994.

Levitus, S., Burgett, R. and Boyer, T. P.: World Ocean Atlas 1994 Volume 3: Nutrients, World Ocean Atlas, 3 [online] Available from: http://data.nodc.noaa.gov/woa/WOA13/DOC/woa13_vol4.pdf (Accessed 21 November 2015), 1994.

Maher, W. and Woo, L.: Procedures for the storage and digestion of natural waters for the determination of filterable reactive phosphorus, total filterable phosphorus and total phosphorus, Anal. Chim. Acta, 375(1-2), 5–47, doi:10.1016/S0003-2670(98)00274-8, 1998.

Mahowald, N., Jickells, T. D., Baker, A. R., Artaxo, P., Benitez-Nelson, C. R., Bergametti, G., Bond, T. C., Chen, Y., Cohen, D. D., Herut, B., Kubilay, N., Losno, R., Luo, C., Maenhaut, W., McGee, K. A., Okin, G. S., Siefert, R. L. and Tsukuda, S.: Global distribution of atmospheric phosphorus sources, concentrations and deposition rates, and anthropogenic impacts, Global Biogeochem. Cycles, 22(4), doi:10.1029/2008GB003240, 2008.

Martino, M., Hamilton, D., Baker, A. R., Jickells, T. D., Bromley, T., Nojiri, Y., Quack, B. and Boyd, P. W.: Western Pacific atmospheric nutrient deposition fluxes, their impact on surface ocean productivity, Global Biogeochem. Cycles, 28(7), 712–728, doi:10.1002/2013GB004794, 2014.

Meybeck, M.: Carbon, Nitrogen, and Phosophorous Transport by World Rivers, Am. J. Sci., 282(4), 401–450, doi:10.2475/ajs.282.4.401, 1982.

Moore, C. M., Mills, M. M., Arrigo, K. R., Berman-Frank, I., Bopp, L., Boyd, P. W., Galbraith, E. D., Geider, R. J., Guieu, C., Jaccard, S. L., Jickells, T. D., La Roche, J., Lenton, T. M., Mahowald, N. M., Marañón, E., Marinov, I., Moore, J. K., Nakatsuka, T., Oschlies, A., Saito, M. A., Thingstad, T. F., Tsuda, A. and Ulloa, O.: Processes and patterns of oceanic nutrient limitation, Nat. Geosci., 6(9), 701–710, doi:10.1038/ngeo1765, 2013.

Moutin, T., Karl, D. M., Duhamel, S., Rimmelin, P., Raimbault, P., Van Mooy, B. A. S. and Claustre, H.: Phosphate availability and the ultimate control of new nitrogen input by nitrogen fixation in the tropical Pacific Ocean, Biogeosciences, 5(1), 95–109, doi:10.5194/bg-5-95-2008, 2008.

Myriokefalitakis, S., Daskalakis, N., Mihalopoulos, N., Baker, A. R., Nenes, A. and Kanakidou, M.: Changes in dissolved iron deposition to the oceans driven by human activity: a 3-D global modelling study, Biogeosciences, 12(13), 3973–3992, doi:10.5194/bg-12-3973-2015, 2015.

Myriokefalitakis, S., Vignati, E., Tsigaridis, K., Papadimas, C., Sciare, J., Mihalopoulos, N., Facchini, M. C., Rinaldi, M., Dentener, F. J., Ceburnis, D., Hatzianastasiou, N., O'Dowd, C. D., van Weele, M. and Kanakidou, M.: Global Modeling of the Oceanic Source of Organic Aerosols, Adv. Meteorol., 2010, 1–16, doi:10.1155/2010/939171, 2010.

Nenes, A., Krom, M. D., Mihalopoulos, N., Van Cappellen, P., Shi, Z., Bougiatioti, A., Zarmpas, P. and Herut, B.: Atmospheric acidification of mineral aerosols: A source of bioavailable phosphorus for the oceans, Atmos. Chem. Phys., 11(13), 6265–6272, doi:10.5194/acp-11-6265-2011, 2011.

Newman, E. I.: Phosphorus inputs to terrestrial ecosystems, J. Ecol., 83(4), 713–726, doi:10.2307/2261638, 1995.

Nickovic, S., Vukovic, A., Vujadinovic, M., Djurdjevic, V. and Pejanovic, G.: Technical Note: High-resolution mineralogical database of dust-productive soils for atmospheric dust modeling, Atmos. Chem. Phys., 12(2), 845–855, doi:10.5194/acp-12-845-2012, 2012.

van Noije, T. P. C., Le Sager, P., Segers, A. J., van Velthoven, P. F. J., Krol, M. C. and Hazeleger, W.: Simulation of

tropospheric chemistry and aerosols with the climate model EC-Earth, Geosci. Model Dev. Discuss., 7(2), 1933–2006, doi:10.5194/gmdd-7-1933-2014, 2014.

Okin, G. S., Baker, A. R., Tegen, I., Mahowald, N. M., Dentener, F. J., Duce, R. A., Galloway, J. N., Hunter, K., Kanakidou, M., Kubilay, N., Prospero, J. M., Sarin, M., Surapipith, V., Uematsu, M. and Zhu, T.: Impacts of atmospheric nutrient deposition on marine productivity: Roles of nitrogen, phosphorus, and iron, Global Biogeochem. Cycles, 25(2), doi:10.1029/2010GB003858, 2011.

Olgun, N., Duggen, S., Langmann, B., Hort, M., Waythomas, C., Hoffmann, L. and Croot, P.: Geochemical evidence of oceanic iron fertilization by the Kasatochi volcanic eruption in 2008 and the potential impacts on Pacific sockeye salmon, Mar. Ecol. Prog. Ser., 488, 81–88, doi:10.3354/meps10403, 2013.

Olson, J.: Major world ecosystem complexes ranked by carbon in live vegetation: A database, Glob. Ecosyst. Database, Version 1, doi:10.3334/CDIAC/lue.ndp017, 1992.

Palandri, J. L. and Kharaka, Y. K.: A compilation of rate parameters of water-mineral interaction kinetics for application to geochemical modeling, Menlo Park. Calif. U.S. Dept. Inter. U.S. Geol. Surv., 64 [online] Available from: http://pubs.usgs.gov/of/2004/1068/ (Accessed 8 March 2016), 2004.

Paytan, A., Cade-Menun, B. J., McLaughlin, K. and Faul, K. L.: Selective phosphorus regeneration of sinking marine particles: evidence from 31P-NMR, Mar. Chem., 82(1-2), 55–70, doi:10.1016/S0304-4203(03)00052-5, 2003.

Powell, C. F., Baker, A. R., Jickells, T. D., Bange, H. W., Chance, R. J. and Yodle, C.: Estimation of the Atmospheric Flux of Nutrients and Trace Metals to the Eastern Tropical North Atlantic Ocean, J. Atmos. Sci., 72(10), 4029–4045, doi:10.1175/JAS-D-15-0011.1, 2015.

Quennehen, B., Raut, J.-C., Law, K. S., Ancellet, G., Clerbaux, C., Kim, S.-W., Lund, M. T., Myhre, G., Olivié, D. J. L., Safieddine, S., Skeie, R. B., Thomas, J. L., Tsyro, S., Bazureau, A., Bellouin, N., Daskalakis, N., Hu, M., Kanakidou, M., Klimont, Z., Kupiainen, K., Myriokefalitakis, S., Quaas, J., Rumbold, S. T., Schulz, M., Cherian, R., Shimizu, A., Wang, J., Yoon, S.-C. and Zhu, T.: Multi-model evaluation of short-lived pollutant distributions over East Asia during summer 2008, Atmos. Chem. Phys. Discuss., 15(7), 11049–11109, doi:10.5194/acpd-15-11049-2015, 2015.

Sesartic, A. and Dallafior, T. N.: Global fungal spore emissions, review and synthesis of literature data, Biogeosciences, 8(5), 1181–1192, doi:10.5194/bg-8-1181-2011, 2011.

Somasundaran, P., Amankonah, J. O. and Ananthapadmabhan, K. P.: Mineral—solution equilibria in sparingly soluble mineral systems, Colloids and Surfaces, 15, 309–333, doi:10.1016/0166-6622(85)80081-0, 1985.

Stohl, A., Aamaas, B., Amann, M., Baker, L. H., Bellouin, N., Berntsen, T. K., Boucher, O., Cherian, R., Collins, W., Daskalakis, N., Dusinska, M., Eckhardt, S., Fuglestvedt, J. S., Harju, M., Heyes, C., Hodnebrog, Ø., Hao, J., Im, U., Kanakidou, M., Klimont, Z., Kupiainen, K., Law, K. S., Lund, M. T., Maas, R., MacIntosh, C. R., Myhre, G., Myriokefalitakis, S., Olivié, D., Quaas, J., Quennehen, B., Raut, J.-C., Rumbold, S. T., Samset, B. H., Schulz, M., Seland, Ø., Shine, K. P., Skeie, R. B., Wang, S., Yttri, K. E. and Zhu, T.: Evaluating the climate and air quality impacts of short-lived pollutants, Atmos. Chem. Phys. Discuss., 15(11), 15155–15241, doi:10.5194/acpd-15-15155-2015, 2015.

Tegen, I., Harrison, S. P., Kohfeld, K., Prentice, I. C., Coe, M. and Heimann, M.: Impact of vegetation and preferential source areas on global dust aerosol: Results from a model study, J. Geophys. Res. Atmos., 107(D21), AAC 14–1–AAC 14–27, doi:10.1029/2001JD000963, 2002.

Tipping, E., Benham, S., Boyle, J. F., Crow, P., Davies, J., Fischer, U., Guyatt, H., Helliwell, R., Jackson-Blake, L., Lawlor, A. J., Monteith, D. T., Rowe, E. C. and Toberman, H.: Atmospheric deposition of phosphorus to land and freshwater, Environ. Sci. Process. Impacts, 16(7), 1608–1617, doi:10.1039/C3EM00641G, 2014.

Tsigaridis, K., Daskalakis, N., Kanakidou, M., Adams, P. J., Artaxo, P., Bahadur, R., Balkanski, Y., Bauer, S. E., Bellouin, N., Benedetti, A., Bergman, T., Berntsen, T. K., Beukes, J. P., Bian, H., Carslaw, K. S., Chin, M., Curci, G., Diehl, T., Easter, R. C., Ghan, S. J., Gong, S. L., Hodzic, A., Hoyle, C. R., Iversen, T., Jathar, S., Jimenez, J. L., Kaiser, J. W., Kirkevåg, A., Koch, D., Kokkola, H., Lee, Y. H., Lin, G., Liu, X., Luo, G., Ma, X., Mann, G. W., Mihalopoulos, N., Morcrette, J.-J., Müller, J.-F., Myhre, G., Myriokefalitakis, S., Ng, N. L., O'Donnell, D., Penner, J. E., Pozzoli, L., Pringle, K. J., Russell, L. M., Schulz, M., Sciare, J., Seland, Ø., Shindell, D. T., Sillman, S., Skeie, R. B., Spracklen, D., Stavrakou, T., Steenrod, S. D., Takemura, T., Tiitta, P., Tilmes, S., Tost, H., van Noije, T., van Zyl, P. G., von Salzen, K., Yu, F., Wang, Z., Wang, Z., Zaveri, R. A., Zhang, H., Zhang, K., Zhang, Q. and Zhang, X.: The AeroCom evaluation and intercomparison of organic aerosol in global models, Atmos. Chem. Phys., 14(19), 10845–10895, doi:10.5194/acp-14-10845-2014, 2014.

Tsigaridis, K., Krol, M., Dentener, F. J., Balkanski, Y., Lathière, J., Metzger, S., Hauglustaine, D. A. and Kanakidou, M.: Change in global aerosol composition since preindustrial times, Atmos. Chem. Phys., 6(12), 5143–5162, doi:10.5194/acp-6-5143-2006, 2006.

Uematsu, M., Toratani, M., Kajino, M., Narita, Y., Senga, Y. and Kimoto, T.: Enhancement of primary productivity in the western North Pacific caused by the eruption of the Miyake-jima Volcano, Geophys. Res. Lett., 31(6), L06106,

doi:10.1029/2003GL018790, 2004.

Vet, R., Artz, R. S., Carou, S., Shaw, M., Ro, C.-U. U., Aas, W., Baker, A., Bowersox, V. C., Dentener, F., Galy-Lacaux, C., Hou, A., Pienaar, J. J., Gillett, R., Forti, M. C., Gromov, S., Hara, H., Khodzher, T., Mahowald, N. M., Nickovic, S., Rao, P. S. P. S. P. and Reid, N. W.: A global assessment of precipitation chemistry and deposition of sulfur, nitrogen, sea salt, base cations, organic acids, acidity and pH, and phosphorus, Atmos. Environ., 93, 3–100, doi:10.1016/j.atmosenv.2013.10.060, 2014.

Vignati, E., Facchini, M. C., Rinaldi, M., Scannell, C., Ceburnis, D., Sciare, J., Kanakidou, M., Myriokefalitakis, S., Dentener, F. and ODowd, C. D.: Global scale emission and distribution of sea-spray aerosol: Sea-salt and organic enrichment, Atmos. Environ., 44(5), 670–677, doi:10.1016/j.atmosenv.2009.11.013, 2010.

van Vuuren, D. P., Edmonds, J., Kainuma, M., Riahi, K., Thomson, A., Hibbard, K., Hurtt, G. C., Kram, T., Krey, V., Lamarque, J.-F., Masui, T., Meinshausen, M., Nakicenovic, N., Smith, S. J. and Rose, S. K.: The representative concentration pathways: an overview, Clim. Change, 109(1-2), 5–31, doi:10.1007/s10584-011-0148-z, 2011.

Wang, R., Balkanski, Y., Boucher, O., Ciais, P., Peñuelas, J. and Tao, S.: Significant contribution of combustion-related emissions to the atmospheric phosphorus budget, Nat. Geosci., 8(1), 48–54, doi:10.1038/ngeo2324, 2014.

Weber, R. J., Guo, H., Russell, A. G. and Nenes, A.: High aerosol acidity despite declining atmospheric sulfate concentrations over the past 15 years, Nat. Geosci., 9(4), 282–285, doi:10.1038/ngeo2665, 2016.

Zamora, L. M., Prospero, J. M., Hansell, D. A. and Trapp, J. M.: Atmospheric P deposition to the subtropical North Atlantic: sources, properties, and relationship to N deposition, J. Geophys. Res. Atmos., 118(3), 1546–1562, doi:10.1002/jgrd.50187, 2013.

Biogeosciences Discuss., doi:10.5194/bg-2016-215, 2016
Manuscript under review for journal Biogeosciences
Published: 8 June 2016

Table 1. Emissions of TP and DP (in Tg-P yr^{-1}) used in the TM4-ECPL model for PAST, PRESENT and FUTURE simulations.

	TM4-ECPL	Biomass Burning	Anthropogenic Combustion	Volcanoes	PBAP	Sea Spay	Soils	Total
TP	PAST	0.014	0.008	0.006	0.195	0.007	1.097	1.328
	PRESENT	0.018	0.043					1.366
	FUTURE	0.022	0.009					1.336
DP	PAST	0.007	0.004	0.006	0.165	0.007	0.106	0.295
	PRESENT	0.009	0.021					0.314
	FUTURE	0.011	0.004					0.299

Table 2. Fluorapatite (FAP) acid dissolution constants used for this study.

Mineral*	pH	K(T) (mol m^{-2} s^{-1})	m	A_{MIN} (m^2 g^{-1})	K_{eq}
FAP	<5.5	$5.75x10^{-6}exp[4.1x10^3(1/298-1/T)]$ [a]	0.81 [a]	10.7 [b] (FAP)	$10^{-23.12}$ [d] (FAP)
	5.5 – 6.5	$6.91x10^{-8}exp[4.1x10^3(1/298-1/T)]$ [a]	0.67 [a]		
	>6.5	$6.53x10^{-11}exp[4.1x10^3(1/298-1/T)]$ [a]	0.01 [a]	80.5 [c] (HAP)	$10^{-20.47}$ [d] (HAP)

a) Guidry and Mackenzie (2003); b) Bengtsson et al. (2007); c) Bengtsson et al. (2009); d) van Cappellen and Berner (1991)

**For HAP dissolution constants, we assume those of FAP as adopted from Guidry and Mackenzie (2003) and corrected based on Palandri and Kharaka (2004) reviewed data (see Sect. 2.2)*

Table 3. Secondary DP sources (in Tg-P yr^{-1}) due to OP ageing contained in biomass burning, anthropogenic combustion, sea-spray and dust as well as apatite acid dissolution contained in dust aerosols for PAST, PRESENT and FUTURE simulations calculated by the TM4-ECPL model.

6	TM4-ECPL	Biomass Burning Ageing	Anthropogenic Combustion Ageing	PBAP Ageing	Sea Spay Ageing	Dust Ageing	
						OP Ageing	*Apatite Dissolution*
DP	PAST	0.003	0.001	0.017	0.0001	0.009	0.068
	PRESENT	0.003	0.005	0.018	0.0001	0.010	0.119
	FUTURE	0.004	0.001	0.018	0.0001	0.010	0.084

Table 4. Global and Oceanic deposition fluxes of TP, DP and BP (in Tg-P yr^{-1}) calculated by the TM4-ECPL model.

Deposition	TM4-ECPL	Global	Ocean
TP	PAST	1.275	0.252
	PRESENT	1.314	0.265
	FUTURE	1.284	0.255
DP	PAST	0.356	0.123
	PRESENT	0.433	0.156
	FUTURE	0.378	0.134
BP	PAST	0.369	0.126
	PRESENT	0.446	0.159
	FUTURE	0.391	0.136

Biogeosciences Discuss., doi:10.5194/bg-2016-215, 2016
Manuscript under review for journal Biogeosciences
Published: 8 June 2016

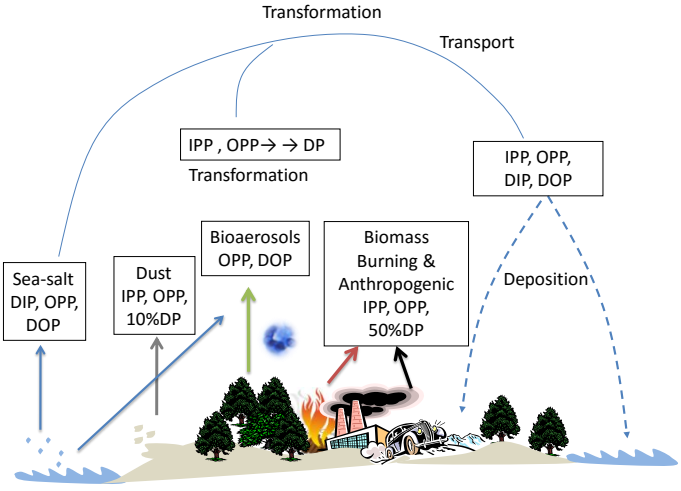

Figure 1. Simplified illustration of the atmospheric P-cycle showing the various sources of particulate IPP, OPP and their dissolved forms (DIP and DOP), the transformation of IP to DP during transport and the deposition of P to the land and to the ocean. Emissions fractions among atmospheric P forms are those used as input in the TM4-ECPL model.

5

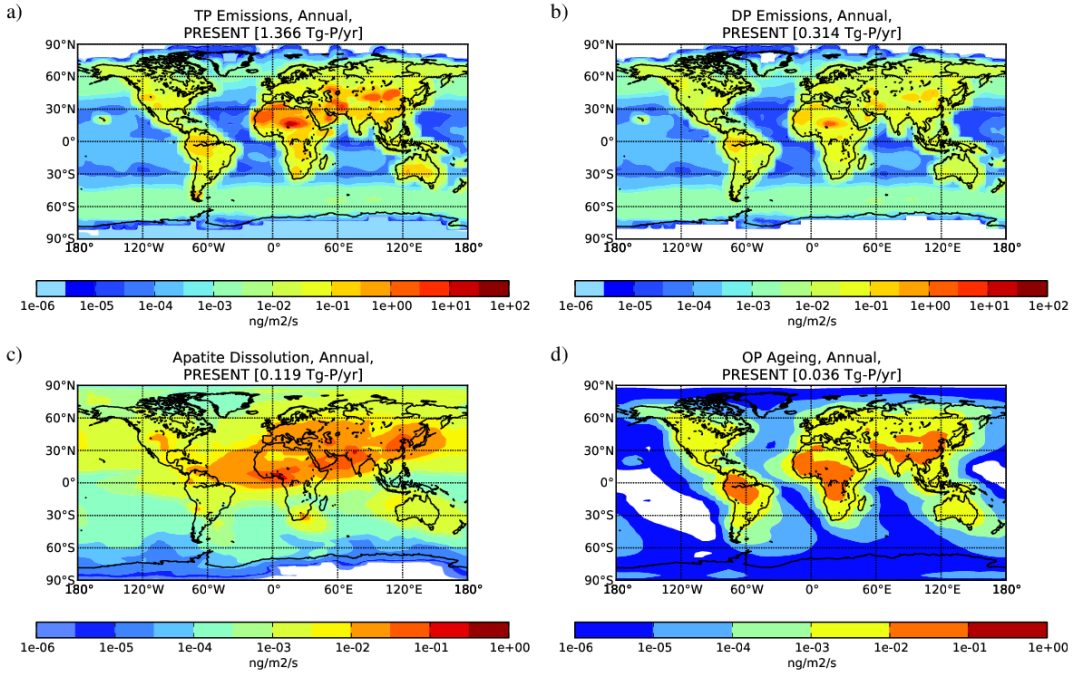

Figure 2. Annual averaged column distributions (in ng-P m^{-2} s^{-1}) of the a) TP emissions b) DP emissions, c) calculated DIP annual acid mobilization fluxes from apatite dissolution and d) DOP production due to OP atmospheric ageing for PRESENT simulation.

Biogeosciences Discuss., doi:10.5194/bg-2016-215, 2016
Manuscript under review for journal Biogeosciences
Published: 8 June 2016

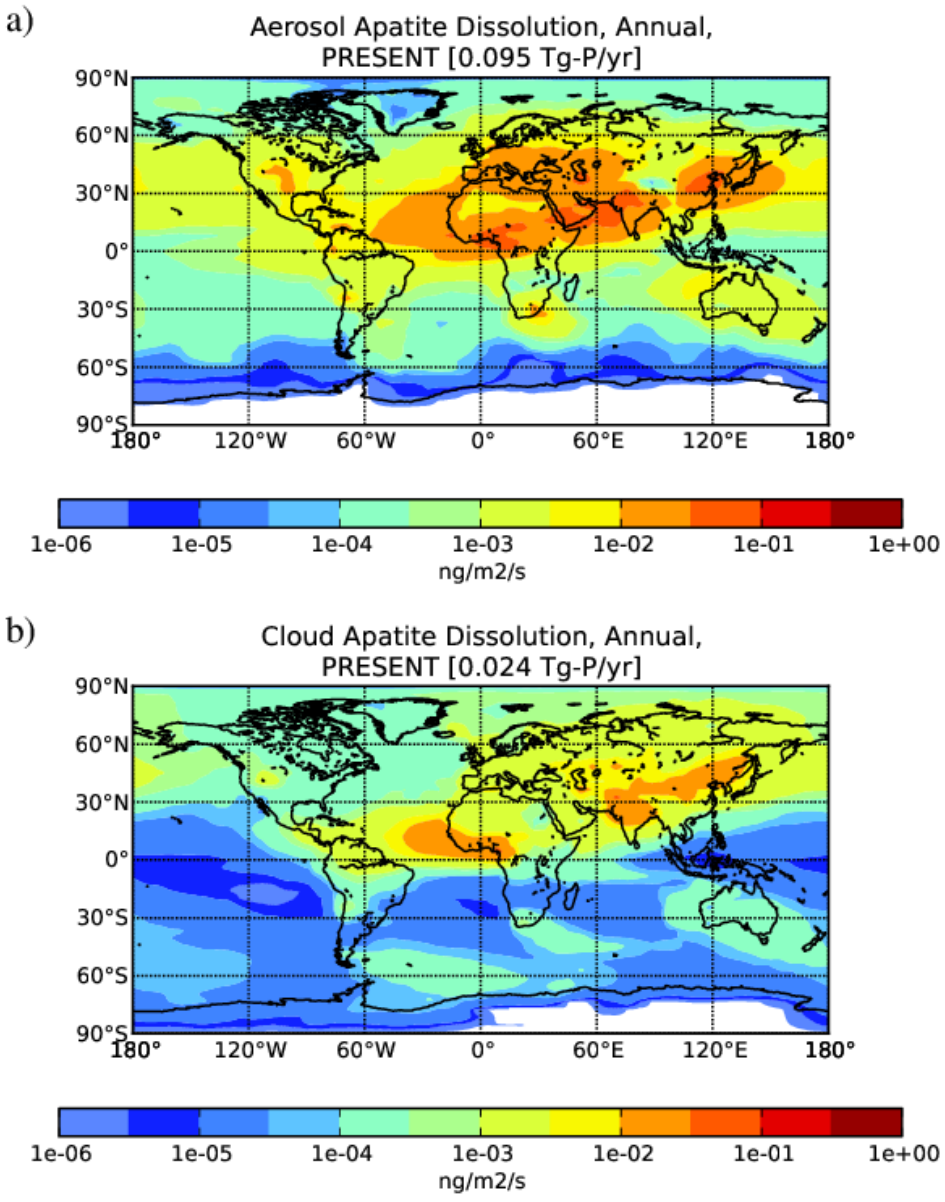

Figure 3. Annual apatite dissolution flux column distributions (in ng-P m^{-2} s^{-1}) a) in aerosol water and b) in cloud droplets, as calculated by the TM4-ECPL for the present atmosphere.

Biogeosciences Discuss., doi:10.5194/bg-2016-215, 2016
Manuscript under review for journal Biogeosciences
Published: 8 June 2016

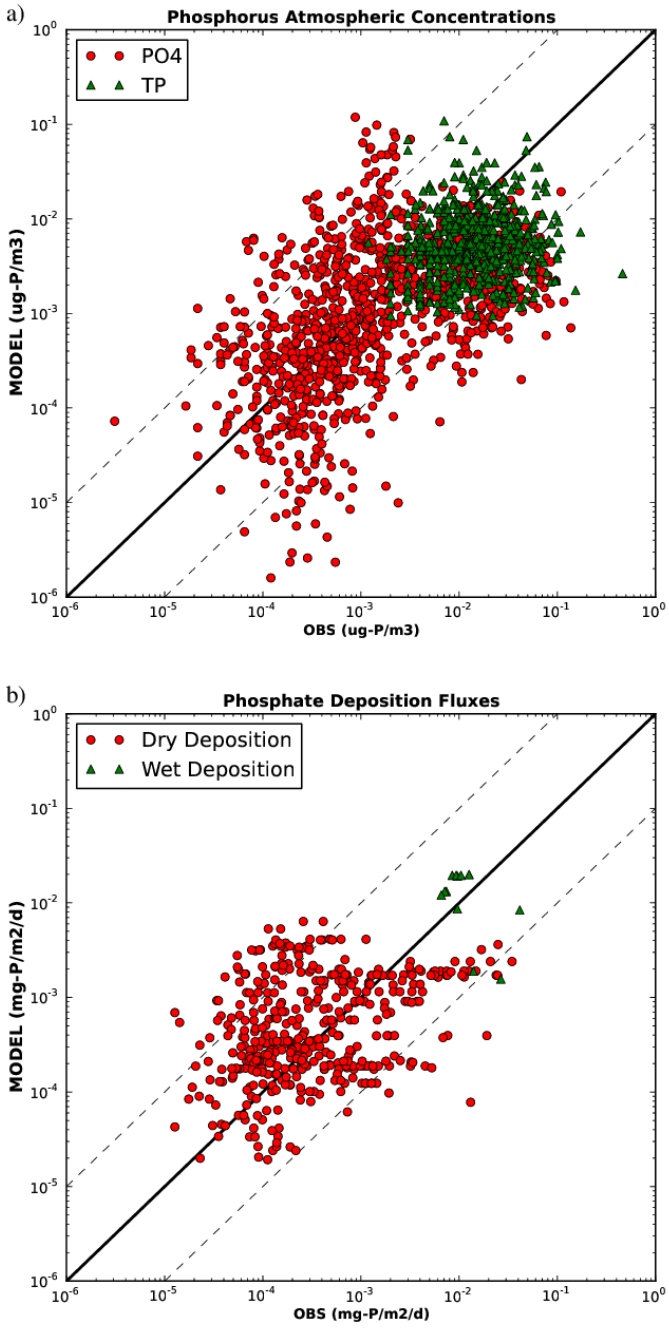

Figure 4. Log-scatter plot of model (y-axis) comparison against observations (x-axis) for a) surface concentrations of TP (red dots) and PO4 (green triangles) and b) dry (red dots) and wet (green triangles) deposition fluxes of PO4. The continuous black line shows the 1:1 correlation and the dashed black lines show the 10:1 and 1:10 relationships, respectively. Atmospheric concentrations are observed by Baker et al. (2010), Martino et al. (2014) and Powell et al. (2015) and from unpublished measurements (Mihalopoulos and co-workers) as observed in the Finokalia Station (35°20′ N, 25°40′ E, Greece) and in the Corsica Island (42°40′ N, 9°04′ E, France). Deposition fluxes are taken from Vet et al. (2014) and from unpublished measurements (Mihalopoulos and co-workers) as observed in the Finokalia Station.

Biogeosciences Discuss., doi:10.5194/bg-2016-215, 2016
Manuscript under review for journal Biogeosciences
Published: 8 June 2016

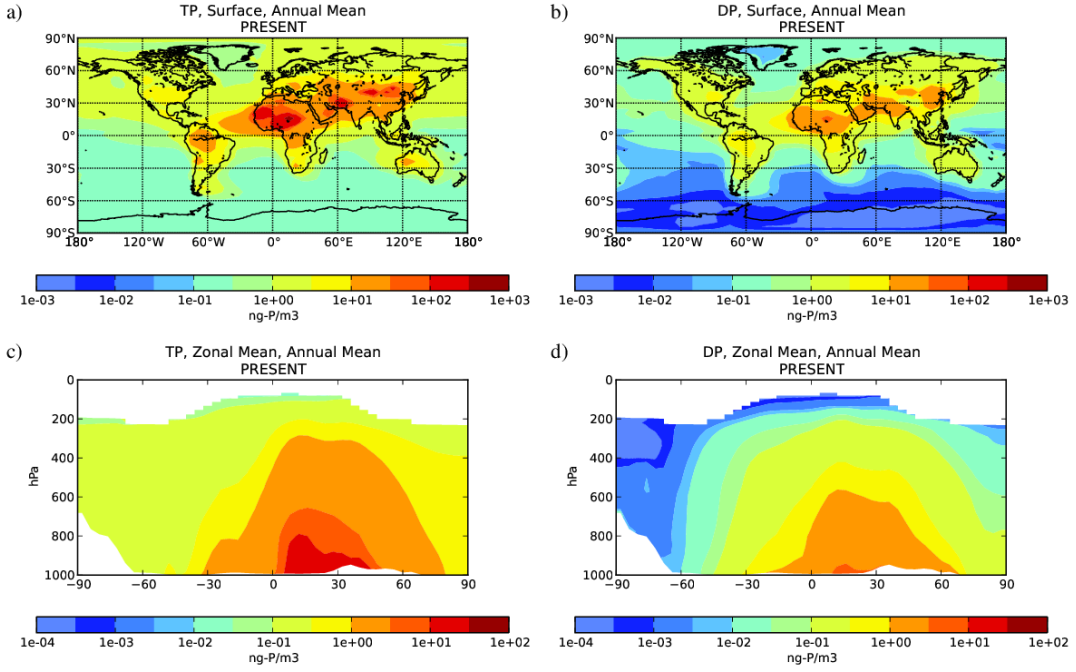

Figure 5. Present day annual mean concentrations (in ng-P m^{-3}) of TP (a, c) and DP (b, d) for the surface (a, b) and in the troposphere as zonal mean (c, d), as calculated by the TM4-ECPL model.

Biogeosciences Discuss., doi:10.5194/bg-2016-215, 2016
Manuscript under review for journal Biogeosciences
Published: 8 June 2016

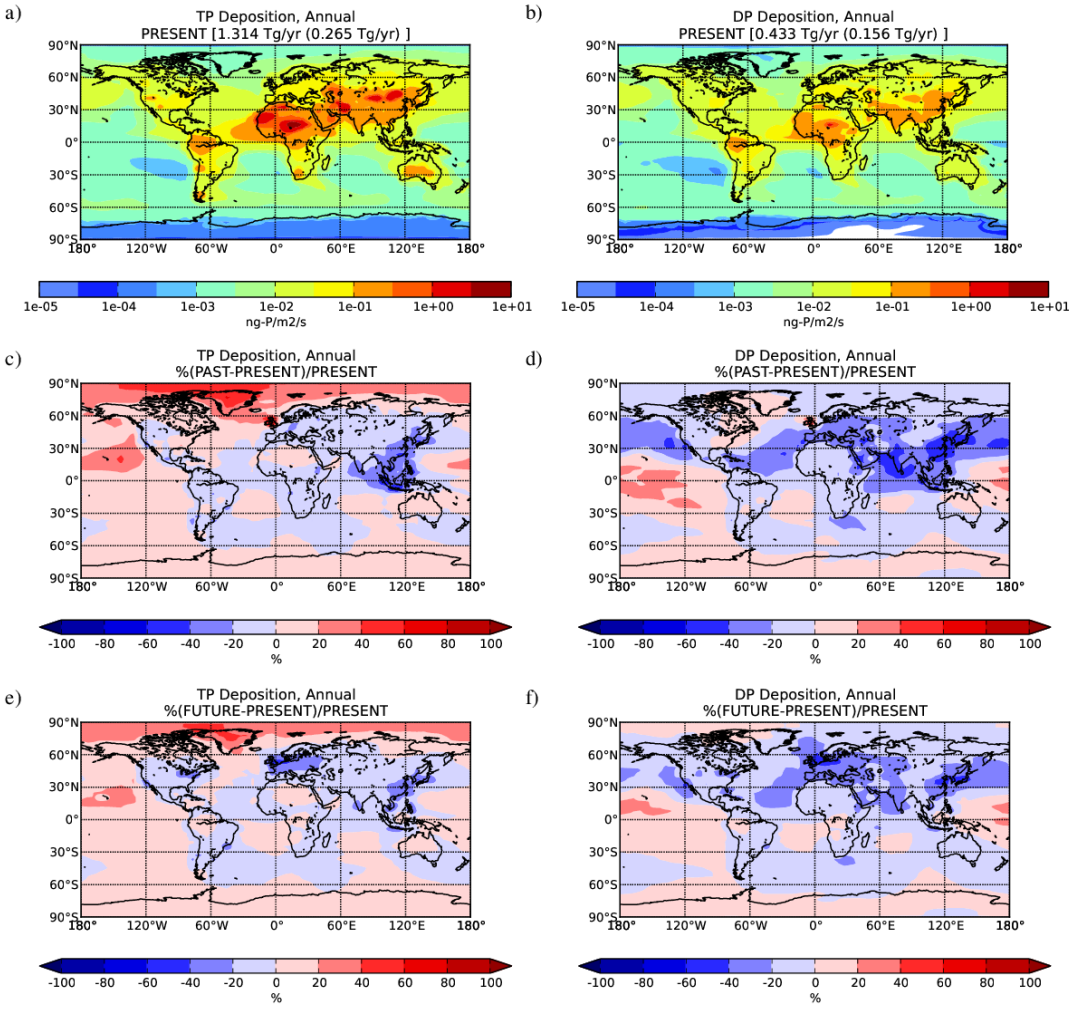

Figure 6. Calculated annual deposition fluxes (in ng-P m^{-2} s^{-1}) for a) TP, b) DP for PRESENT simulation (a,b) and the percentage differences of PAST (c, d) and of FUTURE (e, f) simulations respectively. For the PRESENT annual deposition fluxes (a, b) the global annual fluxes of TP and DP deposition over the globe in brackets (in parentheses only over ocean) are also provided.

5

Biogeosciences Discuss., doi:10.5194/bg-2016-215, 2016
Manuscript under review for journal Biogeosciences
Published: 8 June 2016

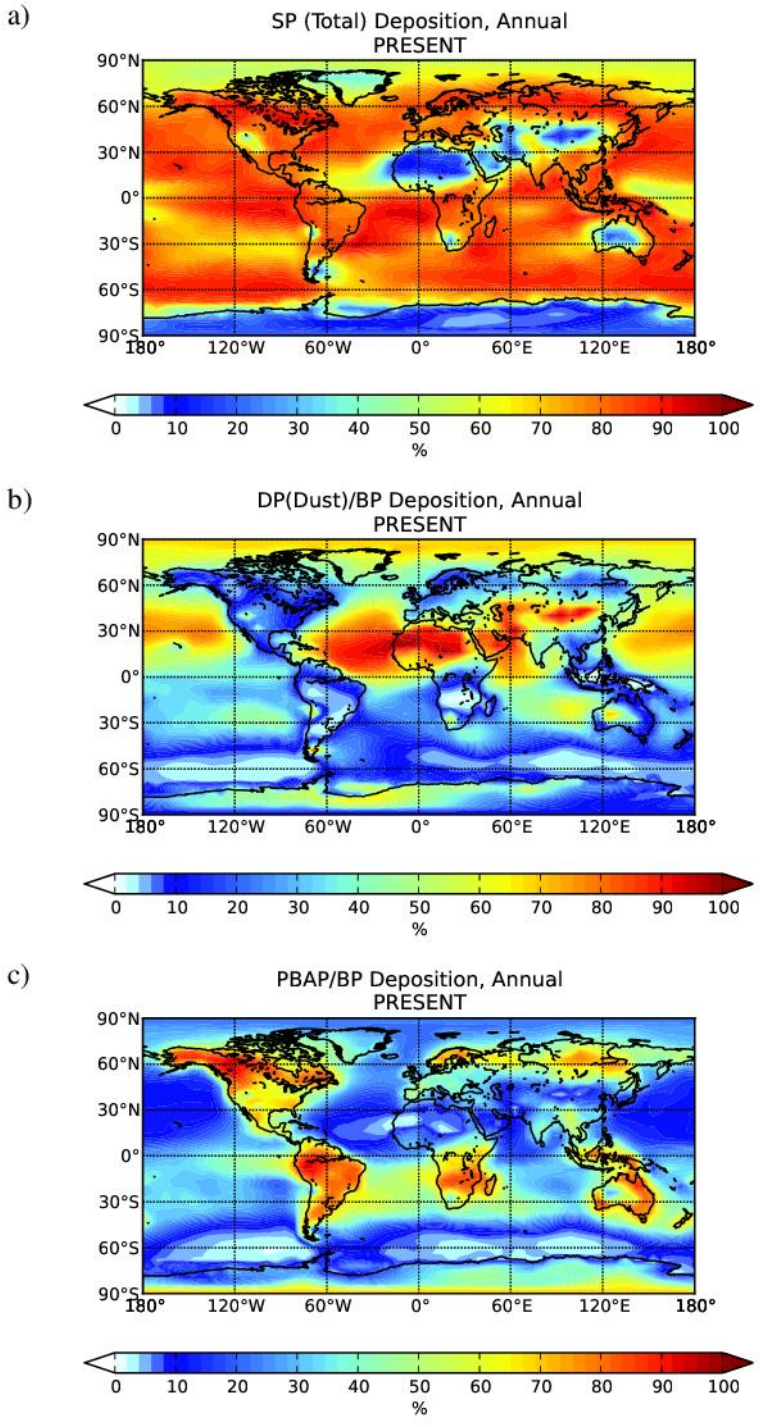

Figure 7. Annual mean percentage fractions in deposited P-containing aerosols of a) P solubility (SP = %DP/TP), b) the relative contribution of DP from dust to the total bioavailable P (BP) and c) the relative contribution of PBAP to BP, as calculated by the TM4-ECPL model for the present atmosphere.